

AD-A084 768

PRINCETON UNIV NJ DEPT OF MECHANICAL AND AEROSPACE --ETC F/8 20/4
EXPERIMENTAL INVESTIGATION OF THREE-DIMENSIONAL SHOCK WAVE TURB--ETC(U)
MAR 80 D S DOLLING, S M BOGDONOFF DAA629-76-6-02969

UNCLASSIFIED

MAE-1468

ARO-14026.2-EX

NL

1 OF 1
AD
A084 768

END

DATE

FORMED

6-80

DTIC

LEVEL II

— ARO 14026.2-EX

(12)

ADA 084768

EXPERIMENTAL INVESTIGATION OF THREE-DIMENSIONAL SHOCK WAVE
TURBULENT BOUNDARY LAYER INTERACTION:

AN EXPLORATORY STUDY OF BLUNT FIN-INDUCED FLOWS

FINAL REPORT

D. S. Dolling
S. M. Bogdonoff

March 1980

ELECTE

U. S. Army Research Office
Grants DAAG29-76-G-0269; 78-G-0140

Gas Dynamics Laboratory
Department of Mechanical and Aerospace Engineering
Princeton University

DDC FILE COPY

Approved for Public Release;
Distribution Unlimited

80 5 FEB 198

UNCLASSIFIED

SECURITY CLASSIFICATION OF THIS PAGE (When Data Entered)

REPORT DOCUMENTATION PAGE		READ INSTRUCTIONS BEFORE COMPLETING FORM
1. REPORT NUMBER	2. GOVT ACCESSION NO.	3. RECIPIENT'S CATALOG NUMBER
	AD-A084768	
4. TITLE (and Subtitle)		5. TYPE OF REPORT & PERIOD COVERED
EXPERIMENTAL INVESTIGATION OF THREE-DIMENSIONAL SHOCK WAVE TURBULENT BOUNDARY LAYER INTERACTION: AN EXPLORATORY STUDY OF BLUNT FIN-INDUCED FLOWS		FINAL REPORT June 1976 - Dec 1979
6. AUTHOR(s)		7. PERFORMING ORG. REPORT NUMBER
David S. Dolling Seymour M. Bogdonoff		MAE-1468
8. PERFORMING ORGANIZATION NAME AND ADDRESS		9. CONTRACT OR GRANT NUMBER(s)
Princeton University, Gas Dynamics Laboratory Mechanical & Aerospace Engineering Department Forrestal Campus, Princeton, NJ 08544		DAAG29-76-G-0269 DAAG29-78-G-0140
11. CONTROLLING OFFICE NAME AND ADDRESS		10. PROGRAM ELEMENT, PROJECT, TASK AREA & WORK UNIT NUMBERS
U. S. Army Research Office Post Office Box 12211 Research Triangle Park, NC 27709		
14. MONITORING AGENCY NAME & ADDRESS (if different from Controlling Office)		12. REPORT DATE
K-156		Mar 1980
		13. NUMBER OF PAGES
		66
		15. SECURITY CLASS. (of this report)
		Unclassified
		15a. DECLASSIFICATION/DOWNGRADING SCHEDULE
16. DISTRIBUTION STATEMENT (of this Report)		
Approved for public release; distribution unlimited 18) ARJ		
17. DISTRIBUTION STATEMENT (of the abstract entered in Block 20, if different from Report)		
NA 19) 14036.2-EX		
18. SUPPLEMENTARY NOTES		
The view, opinions, and/or findings contained in this report are those of the author(s) and should not be construed as an official Department of the Army position, policy, or decision, unless so designated by other documentation.		
19. KEY WORDS (Continue on reverse side if necessary and identify by block number)		
Three-Dimensional Shock Wave-Boundary Layer Interaction Blunt Fin-Induced Interaction Unsteady Flows Turbulent Boundary Layer		
20. ABSTRACT (Continue on reverse side if necessary and identify by block number)		
An experimental study of three-dimensional (3-D) shock wave turbulent boundary layer interaction has been carried out. Interactions generated by fin models having sharp and hemi-cylindrically blunted leading edges have been studied. The emphasis in this particular study was twofold. First, the influence of incoming turbulent boundary layer thickness δ on the streamwise, spanwise and vertical scaling of the interaction was examined. Turbulent boundary layers varying in thickness from .127 cm (.05") to 2.27 cm (.89")		

DD FORM 1473 1 JAN 73

EDITION OF 1 NOV 65 IS OBSOLETE

UNCLASSIFIED

SECURITY CLASSIFICATION OF THIS PAGE (When Data Entered)

UNCLASSIFIED

SECURITY CLASSIFICATION OF THIS PAGE(When Data Entered)

were used. In addition, a study has been conducted to examine the effects of the ratio D/δ (where D is the blunt fin leading edge diameter) on the interaction properties and scaling.

Second, an investigation has been started to examine the unsteady shock wave-boundary layer structure and the resulting high frequency, large amplitude pressure fluctuations which occur ahead of and around the blunt fin leading edge. This is an area which in the past has been largely ignored, yet has important implications, since it is not clear that any mean surface property or flowfield measurements have any real physical significance. To date, measurement techniques and computer software have been developed and exploratory measurements made in the undisturbed turbulent boundary layer and also on the plane of symmetry ahead of the blunt fin. These preliminary measurements, reported on here, are the first phase of a major research program in which this unsteady flowfield structure will be examined in detail.

All of the tests made in the above studies were carried out at a nominal freestream Mach number of 3, a unit Reynolds number of $6.3 \times 10^7 \text{ m}^{-1}$ and under approximately adiabatic wall conditions. This program was carried out during the period 15 June 1976 through December 1979.

Accession For	
NTIS Grant	<input checked="checked" type="checkbox"/>
DOI TAB	<input type="checkbox"/>
Unpublished	<input type="checkbox"/>
Publication	<input type="checkbox"/>
Date	
Institution/	
Availability Codes	
Dist	Available, or special
A	

SECURITY CLASSIFICATION OF THIS PAGE(When Data Entered)

SUMMARY

An experimental study of three-dimensional (3-D) shock wave turbulent boundary layer interaction has been carried out. Interactions generated by fin models having sharp and hemi-cylindrically blunted leading edges have been studied. The emphasis in this particular study was twofold. First, the influence of incoming turbulent boundary layer thickness δ on the stream-wise, spanwise and vertical scaling of the interaction was examined. Turbulent boundary layers varying in thickness from .127 cm (.05") to 2.27 cm (0.89") were used. In addition, a study has been conducted to examine the effects of the ratio D/δ (where D is the blunt fin leading edge diameter) on the interaction properties and scaling.

Second, an investigation has been started to examine the unsteady shock wave-boundary layer structure and the resulting high frequency, large amplitude pressure fluctuations which occur ahead of and around the blunt fin leading edge. This is an area which in the past has been largely ignored, yet has important implications, since it is not clear that any mean surface property or flowfield measurements have any real physical significance. To date, measurement techniques and computer software have been developed and exploratory measurements made in the undisturbed turbulent boundary layer and also on the plane of symmetry ahead of the blunt fin. These preliminary measurements, reported on here, are the first phase of a major research program in which this unsteady flowfield structure will be examined in detail.

All of the tests made in the above studies were carried out at a nominal freestream Mach number of 3, a unit Reynolds number of $6.3 \times 10^7 \text{ m}^{-1}$ and under approximately adiabatic wall conditions. This program was carried out during the period 15 June 1976 through 15 December 1979.

TABLE OF CONTENTS

	<u>Page</u>
SUMMARY	i
TABLE OF CONTENTS	ii
LIST OF FIGURES	iv
NOMENCLATURE	vi
 1 INTRODUCTION	 1
 2 EXPERIMENTAL PROGRAM	 4
2.1 Wind Tunnel Facility	4
2.2 Test Models and Instrumentation	4
2.2.1 General Description	4
2.2.2 Models for D/ δ Study	5
2.2.3 Additional Tests	6
2.3 Unsteady Pressure Measurements	6
2.3.1 Pressure Sensors	6
2.3.2 Data Acquisition System	6
 3 DISCUSSION OF MEAN PRESSURE MEASUREMENTS	 8
3.1 Plane of Symmetry Pressure Distributions and Upstream Influence	 8
3.2 Pressure Distributions Off the Plane of Symmetry	 11
3.2.1 General Description	11
3.2.2 Influence of D/ δ	12
3.3 Fin Pressure Distributions	14
3.3.1 General Description of Fin Leading Edge Pressure Distributions	 14
3.3.2 Effect of Incoming Boundary Layer Thickness on Fin Leading Edge Pressure Distributions	 14
3.3.3 Physical Significance of Fin Height	17
3.4 Fin Body Pressure Distributions	19
3.5 Effects of Leading Edge Geometry on the Plane of Symmetry Pressure Distributions	 20
 4 UNSTEADY PRESSURE MEASUREMENTS	 23
4.1 General Discussion of Program	23
4.2 Measurements in the Undisturbed Boundary Layer	24
4.3 Measurements in the Blunt Fin-Induced Interaction	26

TABLE OF CONTENTS (cont'd)

	<u>Page</u>
5 REMARKS ON THE EXPERIMENTAL OBSERVATIONS	29
REFERENCES	31
TABLE 1	34
FIGURES	35

LIST OF FIGURES

	<u>Page</u>
Figure 1 Schematic of Basic Model Geometry	35
Figure 2 Model 1 and 2 Configurations	36
Figure 3 Coordinate System	37
Figure 4 Schematic of Instrumented Fin	38
Figure 5 Effect of D/δ on the Plane of Symmetry Pressure Distribution	39
Figure 6 Blunt Fin Plane of Symmetry Pressure Distributions	40
Figure 7 Upstream Influence on the Plane of Symmetry as a Function of Mach Number	41
Figure 8 Upstream Influence on the Plane of Symmetry as a Function of D/δ	42
Figure 9 Streamwise Pressure Distributions for $0 \leq Y/D \leq 4$	43
Figure 10 Variation of Peak and Trough Pressures with Y/D	44
Figure 11 Upstream Influence as a Function of D/δ at $Y/D = 1$ and 2	45
Figure 12 Influence of D/δ on Streamwise Pressure Distributions at $Y/D = 1$	46
Figure 13 Influence of D/δ on Peak Pressure Levels	47
Figure 14 Influence of D/δ on Streamwise Pressure Distributions at $Y/D = 2$	48
Figure 15 Typical Fin Leading Pressure Distribution	49
Figure 16 Schematic of Fin Leading Edge Shock Wave Structure	50
Figure 17 Fin Leading Edge Pressure Distributions for Different Incoming Turbulent Boundary Layers	51
Figure 18 Fin Leading Edge Pressure Distributions from Different Studies Plotted versus Z	52
Figure 19 Fin Leading Edge Pressure Distributions from Different Studies plotted versus Z/D	53

LIST OF FIGURES (cont'd)

		<u>Page</u>
Figure 20	Price and Stalling's Fin Leading Edge Pressure Distributions Plotted versus Z/δ	54
Figure 21	Price and Stalling's Fin Leading Edge Pressure Distributions Plotted versus Z/D	55
Figure 22	Schematic of Shock Structure Illustrating Fin Height Needed to Generate "asymptotic" Flowfield	56
Figure 23	Fin Leading Edge ($\phi = 45^\circ$) Pressure Distributions for Different Turbulent Boundary Layers	57
Figure 24	Pressure Distributions at Fin Leading Edge/Body Junction ($\phi = 90^\circ$)	58
Figure 25	Fin Leading Edge Pressure Distributions at $\phi = 0^\circ, 45^\circ$ and 90°	59
Figure 26	Fin Body Pressure Distributions 3.18 cm from Leading Edge	60
Figure 27	Fin Body Pressure Distributions 5.72 cm from Leading Edge	61
Figure 28	Fin Body Pressure Distributions 8.25 cm from Leading Edge	62
Figure 29	Influence of Leading Edge Geometry on the Plane of Symmetry Pressure Distribution	63
Figure 30	Surface Pressure Fluctuation Levels in the Undisturbed Turbulent Boundary Layer	64
Figure 31	Variance of Pressure Fluctuations on the Plane of Symmetry Ahead of Two Different Diameter Blunt Fins	65
Figure 32	Surface Pressure-Time History on Plane of Symmetry 2.9D Ahead of Fin Leading Edge	66

NOMENCLATURE

D	fin leading edge diameter = DIA
h	fin height
ht _p	height of triple point
l _u	upstream influence
M	freestream Mach number
\bar{p}	root mean square fluctuating pressure
PST	undisturbed freestream static pressure
PT2	freestream pitot pressure
PW	wall static pressure
q	freestream dynamic pressure
RE	freestream unit Reynolds number
T _{aw}	adiabatic wall temperature
T _w	wall temperature
U	local velocity in boundary layer
U _e	velocity at boundary layer edge
X	coordinate parallel to the tunnel axis measured from the fin leading edge
XS	distance along instrumentation line measured from the undisturbed freestream shock wave position
Y	coordinate normal to the X-axis in the plane of the test surface measured from the fin leading edge
Z	coordinate normal to the XY plane measured from the fin leading edge/tunnel floor interface
δ	boundary layer thickness at the start of the interaction pressure rise = DELTA
φ	angular position around blunt leading edge, or plane of symmetry shock wave angle
Δ	bow shock wave detachment distance

1. INTRODUCTION

Under the sponsorship of the Army Research Office and other agencies, the Gas Dynamics Laboratory of Princeton University has been carrying out experimental studies of three-dimensional (3-D) shock wave turbulent boundary layer interactions. Specifically, such interactions can occur at wing/fuselage or fin/body junctions on supersonic aircraft and missiles and in many types of engine inlets. Despite their practical significance, both in these specific cases and in the most general sense, few experimental studies have been sufficiently wide ranging and detailed enough to gain any fundamental understanding of the interactions' properties.

In the earliest program carried out at the Gas Dynamics Laboratory, surface property distributions and detailed flowfield measurements were made in an interaction generated by a skewed shock wave. The shock was generated by a sharp leading edged fin model mounted normal to a flat surface (Fig. 1) on which a high Reynolds number, Mach 3, turbulent boundary layer developed. Full details of this investigation, carried out by Oskam, et al, are given in Refs. 1 through 5. Oskam's measurements, now being used as a baseline for comparison with numerical computer codes, were instrumental in clearly showing that some of the early ideas of the flowfield structure were incorrect.

This investigation of the skewed shock interaction answered several controversial questions but also posed many new and puzzling problems. Some of these, such as the effects of incoming boundary layer characteristics, of shock wave strength, and the techniques for scaling the interaction in the streamwise, lateral and vertical directions, have been addressed by more recent studies sponsored by the Army Research Office and Naval Air Systems Command. Additionally, with support from the latter two sponsors, a major study has

been made of interactions generated by hemi-cylindrically blunted fin models. In this case, a detached curved shock wave is generated which interacts with the incoming turbulent boundary layer.

In these experiments carried out over the last 3 years, very detailed surface property measurements have been made over a wide range of incoming boundary layer thicknesses, fin leading edge diameters and angles of attack. Observations and correlations of these data coupled with sparser information from many previous investigators, have revealed properties of the interaction which were not apparent from any one previous study alone. Some elements of these have been presented at recent technical meetings^[6-10].

The measurements from these studies have shown clearly that the 3-D interaction's global scale and characteristic properties are radically different from those seen in 2-D interactions. This is true for both the skewed shock and blunt fin-induced interactions. Parameters having a controlling influence on 2-D interactions have little effect on the 3-D interaction. It appears to be a fundamentally different type of flowfield than that associated with the well known, viscous dominated 2-D interaction.

In the study sponsored by the Army Research Office, emphasis in the first year was placed upon examining the effects of incoming turbulent boundary layer thickness on the scale of the skewed shock wave interaction. A description of the tests and a detailed discussion of the results were presented in an interim technical report^[11] in July 1977. They will not be discussed further in this report, which will deal mainly with work carried out in the last two years of the study.

Data measured in the blunt fin study indicated that the details of the pressure distribution, and perhaps the overall scaling, depended on the ratio

of the fin leading edge diameter to turbulent boundary layer thickness (i.e. D/δ). The small amount of available data from the Princeton study, and others, suggested that these effects would be largest for small D/δ ($< .25$). To examine this in more detail, a set of tests were carried out in which D/δ was systematically changed. This was done by testing different diameter fins in a given incoming turbulent boundary layer. The results from this test series are described in detail in Section 3. Results of these tests have clarified an issue which, in the past, has not been well understood. This is the question of the significance of fin height h on the induced flowfield. Section 3.3.3 presents a simple physical argument which describes the role of h and which satisfactorily explains two apparently conflicting sets of experimental results.

In the blunt fin study, schlieren and shadow photographs showed that the shock wave structure ahead of and around the fin leading edge was highly unsteady. This has also been noted by other investigators^[12-14] but apart from some early transonic studies of Robertson's^[15,16], it has never been examined in any detail. Such unsteadiness has important implications, since it is not clear that any mean or averaged flowfield structure, as is frequently sketched in the literature, has any physical significance. Currently, an exploratory study is being carried out of the surface pressure fluctuations on the plane of symmetry ahead of blunted fins. To date, a major part of the effort has been devoted to the development of the necessary hardware and software. The results obtained so far are presented in Section 4. A more detailed study is planned as part of a future program.

2. EXPERIMENTAL PROGRAM

2.1 Wind Tunnel Facility

The experiments were carried out in Princeton University's 20 cm x 20 cm (8"x8") high Reynolds number, supersonic, blowdown tunnel. This facility uses high pressure air stored at atmospheric temperature and can be operated at stagnation pressures in the range 4×10^5 to $3.4 \times 10^6 \text{ Nm}^{-2}$ (60-500 psia). The nominal freestream Mach number is 3.

All the tests reported on here were made at a stagnation pressure of $6.8 \times 10^5 \text{ Nm}^{-2}$ (100 psia) giving a freestream unit Reynolds number of approximately $6.3 \times 10^7 \text{ m}^{-1}$ ($1.6 \times 10^6 \text{ in}^{-1}$). The models were at near adiabatic wall temperature for all tests.

2.2 Test Models and Instrumentation

2.2.1 General Description

Two basic configurations were used. They are shown in Fig. 2. The Model 1 configuration used the tunnel floor boundary layer. This is a 2-D, fully turbulent, equilibrium boundary layer in which detailed spanwise surveys have been made along the entire length of the test section^[17]. Fins were tested at two streamwise stations. At these, the incoming boundary layers were 1.27 cm (0.5") and 2.03 cm (0.8") thick.

Model 2 used the boundary layer which developed on a horizontal, sharp leading edged flat plate which spanned the tunnel. Fins were tested at two streamwise positions, and, at these, the incoming turbulent boundary layers were 0.13 cm (0.050") and 0.33 cm (.13") thick.

The tunnel floor of the Model 1 study and the flat plate of Model 2 were both instrumented with rows of pressure tapings parallel to the X axis (Fig. 3). The fin models could be translated laterally and longitudinally

relative to these fixed rows such that highly detailed pressure distributions could be obtained. The pressure tappings were sampled using two computer controlled 48 port Model 48J4 Scanivalves equipped with Druck strain gauge transducers. With this on-line system, tabulated and plotted pressure distributions could be obtained immediately following a test.

2.2.2 Models for D/δ Study

Tests were made using fins with hemi-cylindrically blunted leading edges. Six models were tested. Their leading edge diameters (D) were in the range $.102 \text{ cm } (0.040") \leq D \leq 2.54 \text{ cm } (1.0")$. By testing these fins at different locations in either the Model 1 or Model 2 configurations, values of D/δ in the range 0.04 to 3.85 were obtained. One fin ($D = 1.27 \text{ cm}$) was instrumented with six columns of pressure tappings (Fig. 4). Nylon seals of thickness $.13 \text{ cm } (.050")$ and $.250 \text{ cm } (.10")$ were used for sealing the fin base/tunnel floor interface and for doubling pressure tapping density. In all cases, the fin heights were such that the triple point and shock structure near the root were unaffected by any free end effects (i.e. effectively a "semi-infinite" fin).

To obtain adequate resolution of the pressure distributions in the interactions generated by the small diameter (i.e. $D < .33 \text{ cm}$) fins, the following technique was used. One of the pressure tappings on the instrumented floor plate was fitted with a sleeve reducing its diameter to $0.0127 \text{ cm } (0.005")$. During a test, the fin model, which was supported on a sting aligned with the tunnel axis, was moved streamwise relative to this tapping. The fin location relative to the tapping was monitored using a calibrated displacement transducer. The fin was moved very slowly (less than 1 mm/sec) to eliminate pressure lag errors. Checks on repeatability, which were good, were made by driving the fin towards and away from the tapping. The change in the incoming boundary layer

thickness resulting from the streamwise motion of the fin was less than 1%.

2.2.3 Additional Tests

To assess effects of fin leading edge geometry on the plane of symmetry pressure distribution, a brief test program was carried out. A 0.79 cm (0.31") thick fin model, having a flat faced leading edge was progressively hemi-cylindrically blunted from the root up. Results from these experiments are given in Section 3.5.

2.3 Unsteady Pressure Measurements

2.3.1 Pressure Sensors

Kulite pressure sensors are being used for measuring the surface pressure fluctuations. These sensors consist of a miniature silicon diaphragm in which a fully active four arm Wheatstone bridge has been atomically bonded using solid state diffusion. Two different sensor models have been tested. Model XCQ-062-25D, a differential type, has a 0.071 cm (0.028") diameter pressure sensitive area, and a natural frequency of 500 kHz. Model XCR-093-25A is a true absolute, hermetically sealed sensor having a .203 cm (.080") diameter pressure sensitive area and a natural frequency of 200 kHz. Both can be used in the range $0-1.7 \times 10^5 \text{ Nm}^{-2}$ (0-25 psi). To avoid damage, the transducer diaphragms were shielded. The XCQ model was protected by coating the diaphragm with a thin layer of RTV-511. The XCR model was shielded using a perforated screen.

2.3.2 Data Acquisition System

The pressure sensors were connected on-line to a Hewlett-Packard mini-computer via amplifiers and a Preston Scientific GMAD-1 A/D converter. This A/D converter/computer system is capable of sampling rates of up to 500 kHz/channel. Data are taken in blocks of 12,288 points which are dumped to core

by the A/D converter. They are then written onto magnetic tape. Transfer rates from the core to tape are such that several blocks of data can be taken in a few seconds of tunnel run time. A series of computer programs have been written for analysis of the data following a set of tests. Mean values, rms values, variances, probability density distributions and power spectral density estimates can be obtained.

The hardware and computer programs were all checked out using known inputs. This was done by replacing the pressure sensor by a frequency generator and inputting a known frequency and amplitude sine wave (or square wave) whose mean, rms, variance, probability density distribution, etc., could be calculated theoretically.

3. DISCUSSION OF MEAN PRESSURE MEASUREMENTS

The surface pressure distributions reported on in this section were all measured using the conventional technique of a surface orifice connected to a pressure transducer via a connecting tube. Such a system has effectively zero frequency response and thus the measured pressures are mean values. Exploratory measurements, briefly described in Section 4, show that these surface pressures are in fact highly unsteady and that large amplitude fluctuations about the mean exist. This implies that care is needed in using mean surface property distributions in deriving possible flowfield structures, since the derived steady model may have no real physical significance.

3.1 Plane of Symmetry Pressure Distributions and Upstream Influence

Pressure distributions on the plane of symmetry ahead of the fins are shown in Fig. 5. The distance axis X is plotted non-dimensionalized by D , since this correlates, to first order, the interaction scale. Measurements made at Princeton^[6-10] show that the plane of symmetry interaction scale depends predominantly on the fin leading edge diameter and not on the incoming turbulent boundary layer thickness. This is illustrated in Fig. 6, where data from the current study and others are shown. In this data set, the incoming boundary layer thickness varies by 46:1, yet the upstream influence lies between 2.5 and 3- D . In terms of boundary layer thicknesses, the upstream influence for these flows varies from 1 to 11.

Figure 5 shows that although D is the dominant parameter in determining the streamwise scale of the interaction, the details of the pressure distribution depend on the ratio of D/δ . In particular, the upstream pressure peak (labelled P_{pk1} on Fig. 5) increases with increasing D/δ , whereas upstream influence decreases. At the lower end of the D/δ range tested (i.e. ≤ 0.15) the

value of P_{PK1} is about constant, although as D/δ continues to decrease the upstream influence l_u increases. For the smaller diameter fins (i.e., $D \leq .33$ cm), there was some difficulty in accurately measuring the streamwise distance of the fin leading edge from the pressure tapping, but even with errors in X up to $\pm 5\%$ the trends will remain the same.

Interactions of this type, generated by blunted fins, or cylindrical protuberances, have been studied by many investigators^[5-10,12,13,14,18-30]. Surface pressure distributions, heat transfer rate distributions, and surface oil patterns have been taken to determine effects of protuberance geometry and/or freestream and incoming boundary layer conditions on the disturbed flowfield. The main concentration has been on the region on and close to the plane of symmetry. These studies were examined in some detail to see if any data existed which would provide further information on the effects of D/δ on the interaction.

Values of upstream influence (l_u) estimated from the above studies necessarily involves inconsistencies and scatter since they have been obtained using different techniques. Only flowfields induced by semi-infinite fins are considered here. For surface oil patterns, l_u is defined as the distance from the fin base to the upstream oil accumulation line. The current measurements, in which both surface oil patterns and pressure distributions were taken show that l_u from the former is typically 10-20% less than that estimated from the initial pressure rise. Least accurate are the estimates based on heat transfer rate distributions and schlieren or shadow photographs. The problem with the former is not so much the accuracy of the measurements but the poor spatial resolution of the points. Using photographs to determine the intersection point of the plane of symmetry shock wave with the floor is also of

questionable accuracy since the flowfield is highly unsteady and the shock motion is of order $1D$.

Most of these studies were made in the Mach number range $2.5 \leq M \leq 6$ with incoming turbulent boundary layers in the range $.13 \text{ cm } (.050'') \leq \delta \leq 15.24 \text{ cm } (6.0'')$. The upstream influence, shown in Fig. 7 plotted against M , fell between 2 and $4D$. There is controversy over whether l_u depends directly on M . Sedney^[25], observed from oil patterns that in terms of D , l_u increased with increasing Mach number. However, in Sedney's tests, increasing M increased δ , which for a fixed diameter cylinder decreases the ratio D/δ , which, as shown below, tends to increase l_u . Other investigators^[13], who measured detailed centerline pressure distributions over the range $2.3 \leq M \leq 4.44$, with a boundary layer about $15.24 \text{ cm } (6.0'')$ thick, observed no effect of M on l_u . The bow shock stand-off distance Δ depends on M , but for $M > 2$, changes in Δ with M are small, and additionally, Δ is only a small proportion of l_u . Apart from this effect, there appears to be little experimental evidence that the Mach number has a significant effect on l_u .

Close examination of the data plotted in Fig. 7 shows that although D is the dominant parameter in determining l_u , there is a secondary influence of δ as shown in Fig. 8 where the data are replotted as a function of D/δ . The trend of decreasing l_u with increasing D/δ for the whole data set is particularly apparent if experiments such as Westkaempers are examined. No studies could be found for which D/δ was greater than about 10 . The sparse existing data of Fig. 8 suggest that for $D/\delta > \sim 5$, l_u is constant at around $2D$.

It should be emphasized that the above observations on upstream influence are based on experiments in which the incoming boundary layer was fully turbulent.

Recent experiments by Hung and Clauss^[31] at $M = 5$ with an incoming laminar boundary layer show that in this case l_u is of order $10D$. Their measurements also show that the smaller values of upstream influence, in terms of D , occur at the larger values of D/δ . Data from this study show that when the Reynolds number is increased and the boundary layer becomes turbulent, the upstream influence drops to between 2 and $3D$.

3.2 Pressure Distributions Off the Plane of Symmetry

3.2.1 General Description

The characteristic shape of the plane of symmetry pressure distribution extends outboard several diameters. Figure 9 shows streamwise pressure distributions at $Y/D = 0, 1, 2, 3$, and 4 for an incoming boundary layer 1.27 cm (0.5") thick. The fin leading edge diameter in this case is 1.27 cm (0.5"). The plane of symmetry downstream pressure maximum (marked P_{MAX} in Fig. 6), is not reproduced in this figure. The scaling of the pressure axis has been chosen to give the best definition to the distributions in the range $1 \leq Y/D \leq 4$.

Both pressure peaks, particularly the downstream one, decay quickly, and their locations move away from the undisturbed freestream shock wave location ($X_s = 0$). This decay is plotted in detail in Fig. 10. In this case, at a Y/D of between 4 and 5, the two peaks and the trough between them merge. Further outboard, the pressure distribution is characterized by a single peak which decays very gradually, having a pressure ratio of about 1.1 at 50 diameters outboard. Figure 10 shows that the trough pressure level is not strongly affected by increasing Y/D . It maintains a pressure ratio of between 1.25 and 1.4 and is located almost directly underneath the freestream shock wave location.

From Fig. 11, it can be seen that upstream influence in terms of D increases with increasing Y/D . It is possible that this behavior is associated with the ever increasing mass of fluid from the bottom of the incoming boundary layer which is being swept outboard ahead of the shock wave. Referring back to Fig. 9, it can be seen that 4 to 5 diameters downstream of the undisturbed freestream shock wave location ($X_s = 0$), the pressure distributions merge, implying an extensive region with very small lateral pressure gradients. The flowfield structure responsible for this complex behavior is unknown. Several investigators^[12,14,25] have proposed flowfield models based on their surface measurements, in particular surface oil patterns, but these are only speculative. An exploratory investigation of the blunt fin-induced interaction flowfield is planned as the next phase of this study.

3.2.2 Influence of D/δ

Figure 12 shows streamwise pressure distributions measured 1D outboard of the plane of symmetry for six different values of D/δ in the range $0.07 \leq D/\delta \leq 3.85$. The streamwise scale of the interaction correlates well using the leading edge diameter to non-dimensionalize X . There are obvious differences in the details, but in the most general sense, D is a suitable correlation parameter for estimating quantities such as upstream influence, interaction length, peak pressure and trough pressure locations. In an absolute distance scale, upstream influence varies between 0.3 cm (0.12") and 7.6 cm (3.0"), a ratio of about 25, yet in terms of D , l_u lies between 2 and 3D.

The figure shows that the greatest effect of D/δ is its influence on the pressure levels of both of the peaks. It does not appear to result in any systematic influence on their location, except at the lowest values of D/δ (.35, .15, and 0.07) where the upstream peak tends to move closer to the

freestream shock wave location. The decrease in pressure ratio of the two peaks with decreasing D/δ is shown graphically in Fig. 13. The largest changes in pressure ratio occur at the lower end of the D/δ range. This is similar to the behavior of the plane of symmetry upstream influence discussed earlier and shown in Fig. 8. Above a D/δ of about 2 the curves flatten out and above 4 the indication is that little further increase in pressure ratio will occur.

Streamwise pressure distributions 2D outboard of the plane of symmetry for the same six values of D/δ are shown in Fig. 14. There exist some similar trends to those observed at 1D, but there are also some significant differences. Upstream influence in terms of D , shown in Fig. 11, increases with decreasing D/δ as is also observed both at $Y/D = 1$ and on the plane of symmetry. The pressure ratios at the two peaks also increase with increasing D/δ . This is shown in Fig. 13. Both peaks increase at about the same rate and in both cases it is fairly gradual. At the larger two values of D/δ (2.0, 3.85) the pressure ratios differ only by about 2% so that it is doubtful if further increases in D/δ will result in any significant increase. Unlike the pressure distributions at $Y/D = 1$, the downstream pressure peaks for the lower two values of D/δ have become less well-defined. It is doubtful whether in these two cases that this double peaked character will persist much further outboard. Figure 9 showed that for the case $D/\delta = 1.0$, the double-peaked type pressure distribution persisted outboard to about 4-5D. The tentative evidence from Fig. 13 suggests that the outboard location at which the peaks effectively merge may depend on the ratio of D/δ .

3.3 Fin Pressure Distributions

3.3.1 General Description of Fin Leading Edge Pressure Distributions

The instrumented fin (see Fig. 4) was tested with four incoming turbulent boundary layers varying in thickness from 0.13 cm (0.05") to 2.03 cm (.80"). A typical pressure distribution on the most forward section of the leading edge ($\phi = 0^\circ$) is shown in Fig. 15. The pressure axis is the local measured wall pressure non-dimensionalized by the pressure behind the normal shock wave (PT2).

The interaction between the fin bow shock and the plane of symmetry shock results in the formation of a supersonic jet embedded in a subsonic region. A schematic of the shock structure, designated Type IV by Edney^[32], is shown in Fig. 16. The jet Mach number is close to 1 resulting in a small pressure loss across the shock AB. At high Mach numbers the peak impact pressure can be several times the freestream pitot pressure.

From inviscid analysis, the jet impact pressure depends only on the freestream Mach number and the impinging shock strength. Its location, however, depends on the relative magnitudes of the pressures in regions 3 and 4, since the jet may curl up or down. Flows where the shock structure is predominantly in the freestream are amenable to an inviscid analysis. When the structure is fully or partially immersed in the incoming boundary layer, a simple analysis is precluded.

3.3.2 Effect of Incoming Boundary Layer Thickness on Fin Leading Edge Pressure Distributions

In the example shown in Fig. 15 the boundary layer thickness was .13 cm (.050") and the peak pressure location about 1.2 cm (.47") above the floor. The triple point and associated shock structure were thus predominantly outside the boundary layer. The other three cases tested, together with this

example are shown plotted in Fig. 17. For the thickest boundary layer ($\delta = 2.03$ cm) the triple point and shock structure are entirely immersed in the boundary layer. Since both the jet structure and the plane of symmetry shock wave are now forming in a lower Mach number region, the peak pressure and local pressures below this are significantly reduced. A similar behavior is observed with the 1.28 cm thick boundary layer. In this case, most of the shock structure is immersed in the boundary layer but the jet forms just above the edge under approximately freestream flow conditions. The peak pressure is thus little different from that observed in the 0.13 cm and 0.33 cm cases where the shock structure and jet form in the external flow. The two data points close to the peak in the 1.28 cm case indicate that the peak is probably in between them and about 7% higher — this is indicated by the dashed lines on the plot.

Whether or not an incoming turbulent boundary layer should be classified as "thick" or "thin" depends fundamentally on its thickness relative to the fin leading edge diameter, and not on any absolute scale. Thus the peak pressure on the fin, which depends on whether or not the triple point is immersed in the boundary layer, in turn is a function of D/δ . The reasoning for this is as follows: Upstream influence l_u , although depending in a second order way on D/δ , is primarily a function of D . For practical purposes, l_u can, in the majority of cases, be taken as lying between 2 and 3D. Knowing l_u and the plane of symmetry shock wave angle ϕ (this can be estimated with reasonable accuracy using a simple technique outlined in Section 3.3.3) the triple point height can be estimated. ϕ depends strongly on M and weakly on Re . Thus, for a fixed Mach number the triple point height should scale as a function of D , and not depend on δ . Therefore, in the general case, the jet impingement point, which is approximately the triple point height, will be a certain number

of diameters above the fin base and whether or not it will be in or above the boundary layer will depend on the value of D/δ .

The simple argument outlined above, indicating that the triple point height should scale with D is supported by the current study and the measurements of other investigators. Figure 18 shows an example for flows where D/δ is large (i.e., $4.5 < D/\delta < 10$) and the shock structure and triple point are predominantly outside of the boundary layer. Two of the data sets are from the Princeton study, the other two are measurements of Kaufman, et.al. (Ref. 12). Plotted versus distance up the fin Z , as in Fig. 18, the pressure peaks do not coincide. With the distance axis non-dimensionalized by D , as in Fig. 19, the correlation is excellent.

The second example uses the data of Price & Stallings^[13] who measured leading edge ($\phi = 0^\circ$) pressure distributions on two different diameter 12.9° sweptback fins at a Mach number of 4.44. The incoming turbulent boundary layer was 15 cm (6.0") thick. These data, plotted in their original form as a function of Z/δ are shown in Fig. 20. Pressure levels are low since the interaction is immersed in the lower part of the incoming boundary layer. Figure 21 shows the same data with the Z axis scaled by D . The location of local pressure peaks, P_1 and P_2 of Fig. 20, now scale in terms of D . Vertical scaling by δ is clearly inappropriate.

Figures 19 and 21 show that scaling the vertical distance Z by D correlates the peak pressure locations for cases predominantly outside of and fully immersed in the boundary layer respectively. In the Princeton study, a single fin was tested with four different turbulent boundary layers (Fig. 17). These four distributions cover flows in which the triple point and shock structure are partially immersed, fully immersed, or well outside the boundary layer.

In this case, scaling by D , (which will not alter the trends of Fig. 17 since D is the same in all cases) is not very satisfactory. The immersion of the shock structure in a non-uniform incoming flow modifies the leading edge pressure distribution and changes the location of peak pressure.

However, the change in the triple point height is relatively small and to first order it still depends mainly on the fin leading edge diameter (for a given freestream Mach number). This is of great importance from the point of view of estimating whether or not under given conditions a blunt fin, or cylindrical protuberance is high enough to be considered "semi-infinite". From a survey of the literature, it is apparent that there is some confusion concerning the physical significance and importance of the fin (or protuberance) geometric parameters h and D , and the flow parameters δ and M . This problem is addressed in the following section.

3.3.3 Physical Significance of Fin Height

Many experimental studies have been made of the disturbed flowfield induced by a cylindrical protuberance or a hemi-cylindrically blunted fin. The general consensus has been to distinguish small and large protuberances on the basis of their height h relative to the undisturbed incoming boundary layer thickness δ . Several investigators have examined the effects of varying h/δ and it has been noted that the "asymptotic result" occurs quickly for $h > \delta$. The "asymptotic result" occurs when any further increases in protuberance height do not further alter the disturbed flowfield.

However, in the most general sense, the ratio h/δ is of little physical significance in determining whether or not the asymptotic result will occur. Use of this ratio as a correlating parameter for test data has tended to obscure the real nature of this type of flowfield and the parameters which scale it.

Physically, the asymptotic condition is reached when the fin height is such that the flow structure at the root is unaffected by the flow over and around the free-end. This implies that the height is sufficient to ensure that a central region exists which serves to isolate the root and free-end structures (Fig. 22). Such a situation exists when h is greater than about $2 h_{tp}$, where h_{tp} is the height of the asymptotic value of the triple point.

Despite the complexity of the flowfield, a simple technique exists for calculating the approximate asymptotic height of the triple point. This approach was pointed out by Westkaemper^[22] in 1969 and is briefly outlined below. From Fig. 22 it can be seen that from geometrical considerations,

$$h_{tp} = (l_u - \Delta) \tan \phi \quad (1)$$

An estimate for ϕ can be obtained using an expression developed by Truitt^[35] for the pressure rise ΔP occurring in the interaction between a lambda footed bowshock wave and a turbulent boundary layer on a flat plate.

$$\frac{\Delta P}{q} = \frac{K}{(M \cdot \text{Rex})^{0.2}} \quad (2)$$

where q , M , Rex , are the freestream dynamic pressure, Mach number, and local Reynolds number. K , an empirical constant, was found by Truitt to be about 5.6. Knowing M and P , oblique shock tables can be used to obtain ϕ . This technique was tested on eight different experiments in which schlieren photographs had been taken and it was found that ϕ could be predicted to within $\pm 2^\circ$. Some uncertainty exists since a micro-second spark photograph shows only one 'frame' of a shock structure which is known to be unsteady. In

calculating ht_p from Eqt. 1, l_u can be obtained from Fig. 8, or may be taken, with little risk of significant error, as $2.5D$. In this sense, the boundary layer thickness only enters the calculation through its 2nd order effect on the upstream influence l_u .

Use of this simple approach explains several of the anomalies existing in the literature. For example, the asymptotic result was observed by Waltrup^[24] at an h/δ of about 7, whereas Price and Stallings^[13], who tested five fins in the range $0.167 \leq h/\delta \leq 1.667$, found that it had already occurred at the lowest value of h/δ . Waltrup's conditions ($M = 2.2$, $Re = 2.4 \times 10^6$, $\delta = .43$ cm, $D = 1.52$ cm) input to equations 1 and 2 gives $ht_p = 1.9$ cm, or 4.4δ , suggesting that the asymptotic result would occur at about twice this height (i.e. say between $7-9\delta$). As noted above, this was the case. For Price and Stallings' flow conditions ($M = 3.71$, $\delta = 15.24$ cm, $D = 5.08$ cm) the equations give $ht_p = 1.17$ cm, or 0.08δ , so it is not surprising that even at the very low value of $h/\delta = 0.167$ the asymptotic result occurs.

3.4 Fin Body Pressure Distributions

Pressure distributions at $\phi = 45^\circ$ and $\phi = 90^\circ$ for all four boundary layers are shown in Figs. 23 and 24 respectively. At $\phi = 45^\circ$, the distributions retain the character of the $\phi = 0^\circ$ data, but with all pressures reduced by about 30-40%. At this value of ϕ , the peak retains the same Z location as at 0° . At 90° , the flow has expanded such that all pressures are close to the undisturbed freestream static level. In this case, the peaks associated with the jet have entirely disappeared. This is illustrated in Fig. 25, where the $\phi = 0^\circ$, 45° and 90° are plotted together, for one of the turbulent boundary layers.

A feature of the $\phi = 90^\circ$ data of Fig. 24 is that the pressure minimum (marked P_{\min} on the figure) is at approximately the same Z location in all four cases. This highlights a trend which starts to occur at $\phi = 90^\circ$ and continues to become more apparent with increasing distance along the fin body. The trend is that the characteristic features of the pressure distributions, such as local pressure minima and maxima, occur at approximately the same vertical location, independent of the thickness of the incoming boundary layer. In addition, the pressure distributions become progressively closer in terms of absolute pressure levels with increasing distance downstream. This development is shown in Figs. 26, 27 and 28 where pressure distributions measured 3.18 cm, 5.27 cm and 8.25 cm downstream of the leading edge, respectively, are plotted. The strong similarities near the fin-floor junction ($0 < Z < 2$ cm), a region whose height is between 1 and 12δ , indicates a common flowfield structure which does not depend on the incoming boundary layer characteristics.

3.5 Effects of Leading Edge Geometry on the Plane of Symmetry Pressure Distributions

In the early part of this study, there was some question of whether any particular region of the fin leading edge was most important in determining the flowfield structure and characteristics. The interaction's sensitivity to a change in geometry of part of the fin leading edge was unknown. To examine this, a series of tests was carried out using a fin having a flat faced leading edge which was progressively hemi-cylindrically blunted from the root upwards. The fin thickness was .79 cm (0.31"). The vertical extents of the blunting were .2 cm (0.08"), .41 cm (.16"), 2.03 cm (.80") and 4.06 cm (1.6"). A fully hemi-cylindrically blunted fin of the same diameter had been tested in a previous study. In each case, pressure distributions were measured on the plane

of symmetry ahead of the model. These are shown in Figure 29.

Maintaining the same fin thickness but changing the leading edge from a hemi-cylinder to a flat surface effectively doubles the upstream influence. It does not result in any significant changes in the overall characteristics of the pressure distribution. Within experimental accuracy the upstream pressure peak (marked P_1 in Fig. 29) does not change over the range of leading edges. This is in basic agreement with the simple formulation of Truitt's (Equation 2) for the pressure rise resulting from the interaction of a lambda footed bow shock with a turbulent boundary layer. It implies that as the upstream influence increases the mean plane of symmetry shock wave angle remains constant, thus forcing the triple point location higher up the fin leading edge. This means that the protuberance height at which the asymptotic flowfield will be generated is a function of the leading edge geometry. These results show that for a given set of incoming flow conditions the height for the flat faced configuration will be twice that needed for a cylinder.

The measurements show that small changes in the geometry of the leading edge can be important. Hemi-cylindrically blunting the fin over a height of 0.2 cm (0.08") has a fairly significant effect on the upstream part of the pressure distribution. Upstream influence is reduced by about 7%. A surprising result is that there is a measurable effect on the upstream part of the pressure distribution but almost none on the downstream portion. It is not until a more substantial height is rounded that a significant decrease in upstream influence occurs and that the pressures closer to the fin decrease. For a rounded height of 2.03 cm the estimated triple point height is 1.34 cm. The bow shock structure occurring ahead of the flat face above this still exerts a very powerful influence on the interaction length scale. Even when the

rounded height is 4.06 cm, which is approximately four times the triple point height, there is a measurable difference between it and the fully cylindrical case.

4. UNSTEADY PRESSURE MEASUREMENTS

4.1 General Discussion of Program

During the last year, techniques have been developed for measuring high frequency surface pressure fluctuations. To date, some exploratory measurements have been made in an undisturbed turbulent boundary layer and on the plane of symmetry ahead of two different blunt fins. Results of these experiments are described in the following two sections.

Currently, little is known about the unsteady behavior of this type of 3-D flowfield. Its cause, its characteristics, in addition to simpler parameters such as its lateral, longitudinal and vertical extent and their dependence on geometry, flow conditions, etc., are all unknowns. Some investigators, notably Robertson^[15,16], have examined elements of the above and obtained interesting results. These experiments, spanning the transonic regime, were carried out using cylindrical protuberances of various diameters and heights. None of them were high enough to be considered "semi-infinite", which tends to make interpretation of the results more difficult. Robertson speculated that on the plane of symmetry the upstream unsteadiness was caused by an oscillating shock wave driven by the natural turbulent boundary layer fluctuations. Downstream of this, in the region referred to as separated flow, he proposed that the fluctuations were caused by the inherent unsteadiness of a multiple horse-shoe vortex type system.

Qualitatively, according to Robertson, this behavior is similar to that observed in 2-D wedge induced interactions. However, the pressure fluctuations in the so called "separated flow" near the fin root are an order of magnitude higher than those measured in 2-D. If the unsteadiness is driven by the natural fluctuations in the incoming turbulent boundary layer, as proposed by Robertson,

an experiment using a laminar layer would verify this. As far as is known, no such experiments have been carried out.

A literature survey of fluctuating pressure measurements indicates that a significant amount of work has been carried out using undisturbed turbulent boundary layers. Power spectra for attached turbulent boundary layers scale on a Strouhal number basis (i.e. the frequency is normalized by multiplying by a typical length and dividing by a typical velocity). For attached turbulent boundary layers, the normalizing parameters which have been used successfully by various investigators are the freestream velocity U_∞ and the boundary layer thickness δ (or displacement thickness δ^*). This poses the question of which parameters will properly scale the frequencies in the region ahead of and close to the fin. Measurements made earlier at the laboratory show conclusively that the appropriate scaling parameter for mean surface property distributions in this region is the fin leading edge diameter D and not boundary layer thickness. Whether D or δ will satisfactorily scale the spectra may indicate whether or not the fluctuations are basically due to pressure gradient amplified turbulence and thus depend on the character of the incoming layer or whether it is a different phenomenon driven by geometric considerations.

4.2 Measurements in the Undisturbed Boundary Layer

A set of measurements was carried out to determine the surface pressure fluctuations in the upstream undisturbed boundary layer. In the literature, most of the experimental effort has been devoted to incompressible flowfields but there does exist a body of work in compressible flow which can be used for comparison purposes. Figure 30(a), taken from Laganelli, et.al. [34], shows measured values of $\sqrt{\bar{p}}/q_e$ as a function of Mach number M_e over the range $0 \leq M \leq 12$, ($\sqrt{\bar{p}}$ is the root mean square pressure fluctuation and q_e is the dynamic pressure at the boundary layer edge).

Measurements in the present study could only be made at a Mach number of 3 since the tunnel nozzle geometry is fixed. The one point plotted on the figure agrees well with the other data. An alternative way of presenting the experimental data which better represents the magnitude of the pressure fluctuations, is to non-dimensionalize \tilde{p} by P , the local mean static pressure at the wall. In this form, shown also in Fig. 30(b) (and also taken from Laganelli^[34]), the increase in the magnitude of the pressure fluctuations with increasing Mach number is clearly shown. The data point from the present tests agrees well with the adiabatic wall theory of Laganelli, et.al. This was also the wall temperature condition during the test.

During these tests with the undisturbed boundary layer, a problem arose, which as yet has not been entirely satisfactorily explained. It was noticed when the transducer, which is flush mounted in a circular wall plug, was rotated about its axis. Such a rotation should not produce any change in the measurements. In this case, the mean pressure value, as well as the rms level of the fluctuations, changed depending on the rotational position. In this high Reynolds number boundary layer, velocities of the fluid close to the wall are very high and the sonic height is only a few thousandths of an inch off the wall. It is possible, that very slight disturbances at the wall, caused by the transducer surface not being perfectly flush, or not being sufficiently smooth, can result in significant changes in the measured fluctuations. This behavior occurred with the two transducers whose diaphragms were protected using a thin RTV-511 rubber film. It did not occur using the third transducer, whose diaphragm is protected using a perforated shield. Under a magnifying glass, pitting of the rubber film could be seen whereas the shield had almost no significant surface irregularities. Currently the rubber film covered

sensors are being re-coated, with great care being taken to ensure a good surface finish.

4.3 Measurements in the Blunt Fin-Induced Interaction

A preliminary set of measurements has been made of the pressure fluctuations on the plane of symmetry ahead of two different blunted fin models. The leading edge diameters were 1.27 cm (0.5") and 2.54 cm (1.0"). In both cases the fin model was located at the same streamwise location in the Model 1 configuration. The incoming boundary layer was 1.27 cm thick.

Figure 31 shows the variance of the pressure fluctuations ahead of the two fins. For clarity the individual data points have been joined by straight lines. There is clearly a need for more data points in the region $-3 \leq X/D \leq -2$, since it is unlikely that the peak and its location are adequately defined. Two data points, one for each fin, have not been plotted on Fig. 31, since the pressure scale was chosen to give the best definition to the bulk of the data. Both points were at $X/D = -0.25$, which is just ahead of the fin root. The measured variance was 10 for the 1.27 cm (0.5") diameter fin and about 12 for the 2.54 cm (1.0") diameter fin. These figures are only approximate since the pressure levels tended to saturate the sensor. It is possible that the true variances are higher. At this location, the variances are about four orders of magnitude higher than the undisturbed boundary layer. However, the root mean square of the pressure fluctuations normalized by the local mean pressure, which gives a better idea of the magnification of the fluctuations, is about 20 times that in the undisturbed boundary layer.

The shape of these curves is similar to that observed by Robertson. The upstream peak in the variance, occurring around $X/D = -2.5$, is just downstream of the initial rise in the mean pressure distribution. This local peak, caused

by random motion of the plane of symmetry shock wave(s), should define approximately the mean shock wave location. Both fins have the same value of the variance at $X/D = -2.5$. Based solely on the one data point, this implies a similar strength shock wave in both cases. This same local peak is also observed ahead of the separated flow region in 2-D wedge and forward facing step generated interactions.

Downstream of this region of shock wave motion, the fluctuation level progressively rises over a streamwise distance of about one diameter. In this region, $-2 \leq X/D \leq -1$, the mean pressure distributions are rather flat and consequently the streamwise (and transverse) pressure gradients are small, such that large excursions of the mean structure would not result in significant pressure changes. In both cases, a second peak also occurs at an X/D of -1 , which in the mean pressure distribution corresponds to a location just ahead of the pressure trough. At the trough, which approximately spans the region $-1 \leq X/D \leq 0.5$, the mean pressure changes are again small, yet the variance increases steeply in the downstream direction. There is presently no satisfactory explanation for this phenomenon. It appears that close to the fin leading edge (i.e., $X/D \sim -1$) the fluctuation levels depend on leading edge diameter.

Power spectra calculated at different locations on the plane of symmetry did not indicate any concentrations of energy around any specific frequency ranges, but displayed a broad band nature like that of the undisturbed boundary layer. In particular, the motion of the plane of symmetry shock wave appears to be effectively random, and Robertson's speculation that it is driven by the natural turbulent boundary layer fluctuations may be correct. A surface pressure/time history plot, consisting of 6144 data points, is shown in Fig. 32.

At this location, 2.9D ahead of the fin leading edge, the pressure trace closely resembles that of the undisturbed boundary layer with a series of "spikes" superimposed on top. These pressure spikes do not feed forward very frequently (i.e., in the figure shown the rate is about 80 per second) but, when they do, their duration is short, typically being a few micro-seconds.

The unsteady measurements reported on very briefly in this section are the beginnings of a major study of the causes and characteristics of the pressure fluctuations in the unsteady flowfield ahead of, and around, the fin root. In an upcoming study, the lateral, longitudinal and vertical extents of the unsteady region and its dependence on fin leading edge diameter and incoming turbulent boundary layer properties will be studied.

5. REMARKS ON THE EXPERIMENTAL OBSERVATIONS

The experimental investigation reported on here is part of a series of studies of 3-D shock wave turbulent boundary layer interactions which has been carried out over the last few years at the Gas Dynamics Laboratory of Princeton University. Interactions generated by fin models with different leading edge geometries have been studied. Measurements made have ranged from detailed surface pressure distributions for all geometries to full flowfield surveys in the case of the sharp leading edged fin. The emphasis in the study in this report is in two main areas. First, the influence of incoming turbulent boundary layer thickness, δ , on the streamwise, spanwise and vertical scaling of the interaction was examined. Second, and this is a critical area in which work has only recently begun, is an investigation of the causes and characteristics of the highly unsteady shock wave boundary layer structure in the blunt fin-induced interaction.

This series of studies, covering a wide range of test geometries and turbulent boundary layers, has generated an extremely detailed surface property data set. This has provided much needed basic information on the significance of different geometric and flow parameters on the interactions' scale and characteristics. These data have been instrumental in showing many of the important differences between 2-D and 3-D interactions. For example, shock wave strength and turbulent boundary layer thickness are both controlling parameters of the streamwise scale of 2-D interactions yet have little effect on the streamwise scale of the 3-D case. However, although a number of parameters have been identified and their effects documented, there still remain many fundamental questions.

Many of these have arisen from studies of the blunt fin-induced interaction. A key item missing is a clear picture of the physical structure of the interaction. Inferring a flowfield model from mean surface property distributions, in particular from surface oil patterns, as has been done by earlier investigators, can lead to misleading conclusions. This was demonstrated by Oskam, et.al., in the early study of the interaction flowfield generated by a sharp leading edged fin. In the blunt fin case, determining the flowfield is further complicated by the highly unsteady behavior of the shock wave - boundary layer structure. In addition, and most importantly, this unsteadiness casts doubt on the real physical significance of any mean, or averaged flowfield structure which may be devised.

The blunt fin-induced interaction structure, which is intimately related to the unsteadiness of the flowfield, will be the main topic addressed in an experimental program planned for the near future. An investigation of the causes and characteristics of the unsteadiness will be made. Its lateral, longitudinal and vertical extents and their dependence on the fin leading edge geometry and turbulent boundary layer properties are all unknowns and will be experimentally determined. In addition, instrumentation and techniques will be developed suitable for exploratory investigation of different regions of the flowfield.













REFERENCES

1. Oskam, B., Vas, I. E. and Bogdonoff, S. M., "An Exploratory Study of a Three-Dimensional Shock Wave Boundary Layer Interaction at Mach 3," Presented at the AGARD Symposium on "Flow Separation", May 1975, Report 1227.
2. Oskam, B., Bogdonoff, S. M. and Vas, I. E., "Study of Three-Dimensional Flow Fields Generated by the Interaction of a Skewed Shock Wave with a Turbulent Boundary Layer," AFFDL-TR-75-21, Final Report, February 1975. Also AMS Report 1264.
3. Oskam, B., Vas, I. E. and Bogdonoff, S. M., "Oblique Shock Wave/Turbulent Boundary Layer Interactions in Three Dimensions at Mach 3 - Part 1," AFFDL-TR-76-48, Final Report, June 1976. Also AMS Report 1292.
4. Oskam, B., Vas, I. E. and Bogdonoff, S. M., "Mach 3 Oblique Shock Wave/Turbulent Boundary Layer Interactions in Three Dimensions," AIAA Paper No. 76-336, July 1976.
5. Oskam, B., "Three-Dimensional Flow Fields Generated by the Interaction of a Swept Shock Wave with a Turbulent Boundary Layer," Princeton University Gas Dynamics Laboratory Report No. 1313. Also Ph.D. Thesis, Aerospace and Mechanical Sciences Department, Princeton University, December 1976.
6. Dolling, D. S., Cosad, C. D. and Bogdonoff, S. M., "Three-Dimensional Shock Wave Turbulent Boundary Layer Interactions - A Preliminary Analysis of Blunted Fin-Induced Flows," Report 1354, MAE Dept., Princeton University, October 1977.
7. Dolling, D. S., Cosad, C. D. and Bogdonoff, S. M., "Three-Dimensional Shock Wave Turbulent Boundary Layer Interactions - A Parametric Study of Blunt Fin-Induced Flows," AIAA Paper No. 78-159, January 1978.
8. Dolling, D. S., Cosad, C. D. and Bogdonoff, S. M., "Three-Dimensional Shock Wave Turbulent Boundary Layer Interactions - A Preliminary Analysis of Blunted Fin-Induced Flows," Boundary Layer Effects - Proceedings of the 7th U. S. Air Force/Federal Republic of Germany Data Exchange Agreement Meeting, AFFDL TR-78-111, September 1978.
9. Dolling, D. S., Cosad, C. D. and Bogdonoff, S. M., "An Examination of Blunt Fin-Induced Shock Wave Turbulent Boundary Layer Interactions," AIAA Paper No. 79-0068, January 1979.
10. Dolling, D. S. and Bogdonoff, S. M., "Some Observations on the Anomalous Behavior of Fin-Induced Shock Wave Turbulent Boundary Layer Interactions," Proceedings of 4th U. S. Air Force/Federal Republic of Germany "Data Exchange Agreement Meeting - Viscous and Interacting Flow Field Effects," BMVg-FBWT 79-31, April 1979.

11. Dolling, D. S., Cosad, C. D., Bogdonoff, S. M. and Vas, I. E., "A Three-Dimensional Study of Fin-Induced Shock Wave Turbulent Boundary Layer Interaction," Interim Technical Report, 15 July 1977, U. S. Army Research Office Grant DAAG29-76-G-0269.
12. Kaufman, L. G., Korkegi, R. H. and Morton, L. C., "Shock Impingement Caused by Boundary Layer Separation Ahead of Blunt Fins," ARL 72-0118, August 1972.
13. Price, A. E. and Stallings, R. L., "Investigation of Turbulent Separated Flows in the Vicinity of Fin Type Protuberances at Supersonic Mach Numbers," NASA TN D-3804, February 1967.
14. Winkelmann, A. E., "Experimental Investigations of a Fin Protuberance Partially Immersed in a Turbulent Boundary Layer at Mach 5," NOLTR-72-33, January 1972.
15. Robertson, J. E., "Characteristics of the Static- and Fluctuating-Pressure Environments Induced by Three-Dimensional Protuberances at Transonic Mach Numbers," Wyle Laboratories Research Staff Report WR 69-3, June 1969.
16. Robertson, J. E., "Prediction of In-Flight Fluctuating Pressure Environments Including Protuberance Induced Flow," Wyle Laboratories Research Staff Report WR 71-10.
17. Fernholz, H. H. and Finley, P. J., "A Critical Compilation of Compressible Turbulent Boundary Layer Data," AGARD-AG-223, June 1977.
18. Lucas, E. J., "Investigation of Blunt Fin-Induced Flow Separation Region on a Flat Plate at Mach Numbers 2.5 to 4.0," AEDC-TR-70-265, January 1971.
19. Uselton, J. C., "Fin Shock-Boundary Layer Interaction Tests on a Flat Plate with Blunted Fins at $M = 3$ and 5," AEDC-TR-67-113, June 1967.
20. Burbank, P. B. and Strass, H. K., "Heat Transfer to Surfaces and Protuberances in a Supersonic Turbulent Boundary Layer," NACA RM L58E01a, July 14, 1958.
21. Burbank, P. B., Newlander, R. A. and Collins, I. K., "Heat-Transfer and Pressure Measurements on a Flat-Plate Surface and Heat Transfer Measurements on Attached Protuberances in a Supersonic Turbulent Boundary Layer at Mach Numbers of 2.65, 3.51, and 4.44," NASA TN D-1372, December 1962.
22. Westkaemper, J. C., "Turbulent Boundary Layer Separation Ahead of Cylinders," AIAA J., Vol. 6, No. 7, pp. 1352-1355, July 1968.
23. Miller, W. H., "Pressure Distributions on Single and Tandem Cylinders Mounted on a Flat Plate in Mach Number 5.0 Flow," Univ. of Texas, Defense Research Laboratory, DRL 538, 1 June 1966.

24. Waltrup, P. J., Hall, D. G. and Schetz, J. A., "Flowfield in the Vicinity of Cylindrical Protuberances on a Flat Plate in Supersonic Flow," AIAA Journal of Spacecraft, Vol. 5, No. 1, January 1968, pp. 127-128.
25. Sedney, R. and Kitchens, C. W., "The Structure of Three-Dimensional Separated Flows in Obstacle-Boundary Layer Interactions," Ballistic Research Laboratories Report No. 1791, June 1975.
26. Sedney, R. and Kitchens, C. W., "Separation Ahead of Protuberances in Supersonic Turbulent Boundary Layers," Ballistic Research Laboratories Report No. 1958, February 1977.
27. Sedney, R. and Kitchens, C. W., "Separation Ahead of Protuberances in Supersonic Turbulent Boundary Layers," AIAA J., Vol. 15, No. 4, April 1977, pp. 546-552.
28. Price, E. A., Howard, P. W. and Stallings, R. L., "Heat Transfer Measurements on a Flat Plate and Attached Fins at Mach Numbers of 3.51 and 4.44," NASA TN-D-2340, June 1964.
29. Gillerlain, J. D., "Fin-Cone Interference Flow Field," AIAA Paper No. 79-0200, January 1979.
30. Voitenko, D. M., Zubkov, A. E. and Panov, Yu.A., "Supersonic Gas Flow Past a Cylindrical Obstacle on a Flat Plate," Mekhanika Zhidkosti i Gaza, Vol. 1, No. 1, pp. 121-125, 1966.
31. Hung, F. T. and Clauss, J. M., "Three-Dimensional Protuberance Interference Heating in High Speed Flow," AIAA Paper No. 80-0289, January 1980.
32. Edney, B., "Anomalous Heat Transfer and Pressure Distributions on Blunt Bodies at Hypersonic Speeds in the Presence of an Impinging Shock," Aeronautical Research Institute of Sweden, Report 115, February 1968.
33. Couch, L. M., "Flow Field Measurements Downstream of Two Protuberances on a Flat Plate Submerged in a Turbulent Boundary Layer at Mach 2.49 and 4.44," NASA TN-D-5297, July 1969.
34. Laganelli, A. L., Martelluci, A. and Shaw, L., "Prediction of Surface Pressure Fluctuations in Hypersonic Turbulent Boundary Layers," AIAA Paper No. 76-409, July 1976.
35. Truitt, R. W., "Hypersonic Turbulent Boundary-Layer Interference Heat Transfer in Vicinity of Protuberances," AIAA J., Vol. 3, No. 9, September 1965, pp. 1754-1755.

TABLE 1

Symbol	Reference	Technique for Estimating l_u
	Lucas [Ref. 18]	Pressure Distribution
	Usselton [Ref. 19]	Pressure Distribution
	Kaufmann, Korkegi & Morton [Ref. 12]	Pressure Distribution
	Winkelmann [Ref. 14]	Pressure Distribution
	Burbank and Strass [Ref. 20]	Heat Transfer Distribution
	Price and Stallings [Ref. 13]	Pressure Distribution
	Burbank, Newlander and Collins [Ref. 21]	Heat Transfer Distribution
	Westkaemper [Ref. 22]	Surface Oil Pattern
	Dolling, Cosad and Bogdonoff [Ref. 9]	Pressure Distribution
	Miller [Ref. 23]	Schlieren Photograph
	Waltrup [Ref. 24]	Schlieren Photograph
	Sedney and Kitchen [Ref. 26]	Surface Oil Pattern

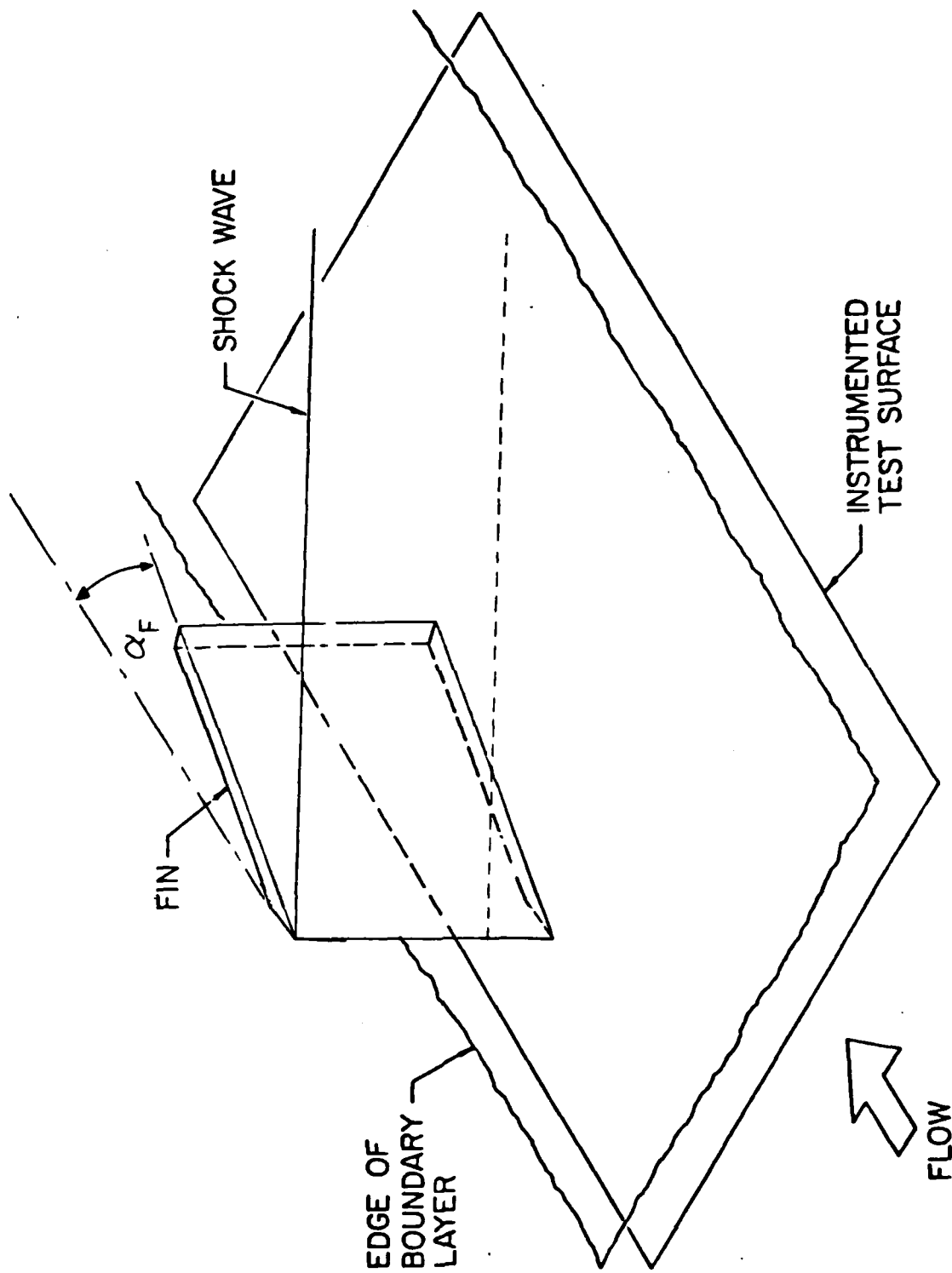


FIGURE 1. Schematic of Basic Model Geometry

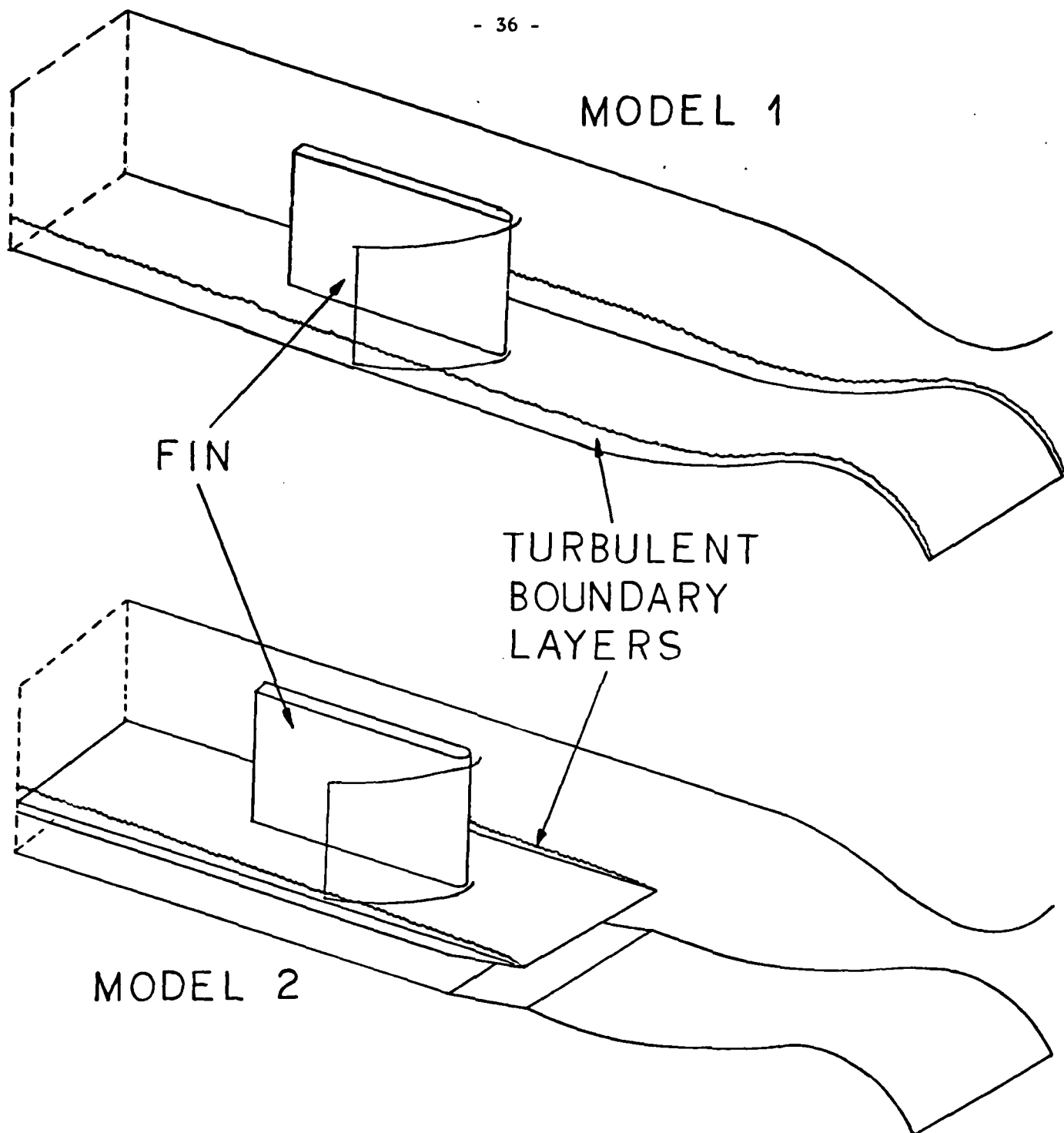


FIGURE 2. Model 1 and 2 Configurations

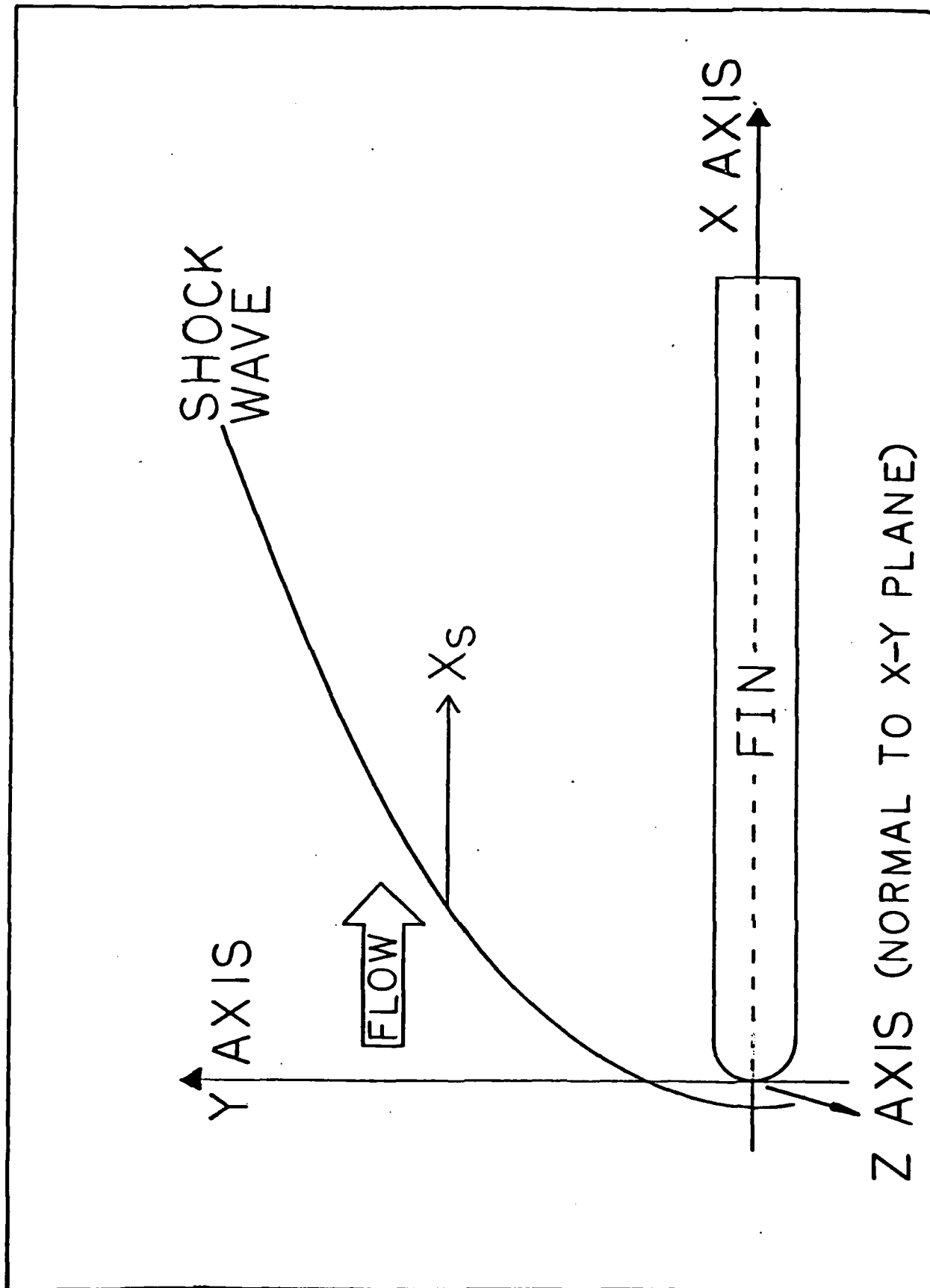


FIGURE 3. Coordinate System.

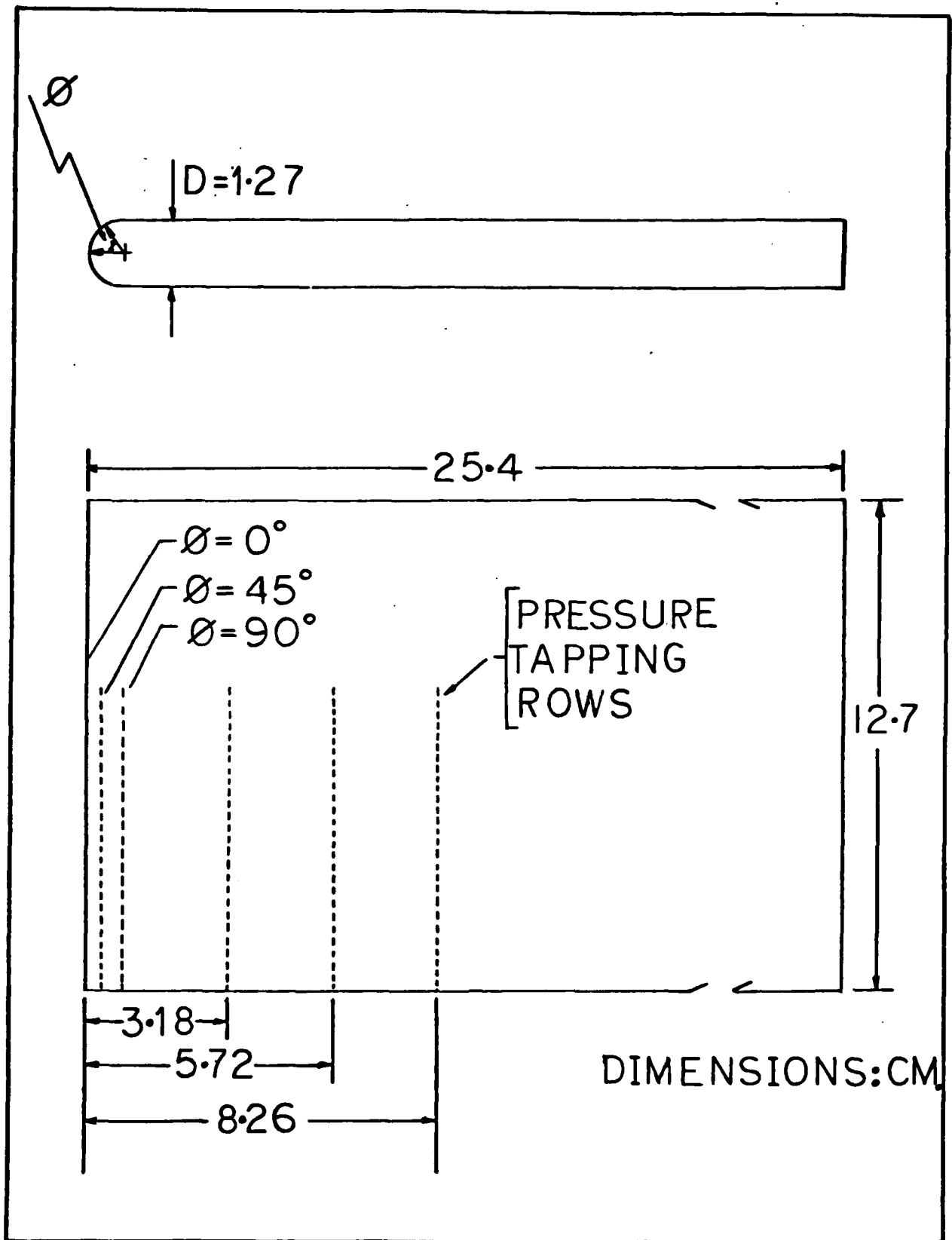


FIGURE 4. Schematic of Instrumented Fin.

29/02/80

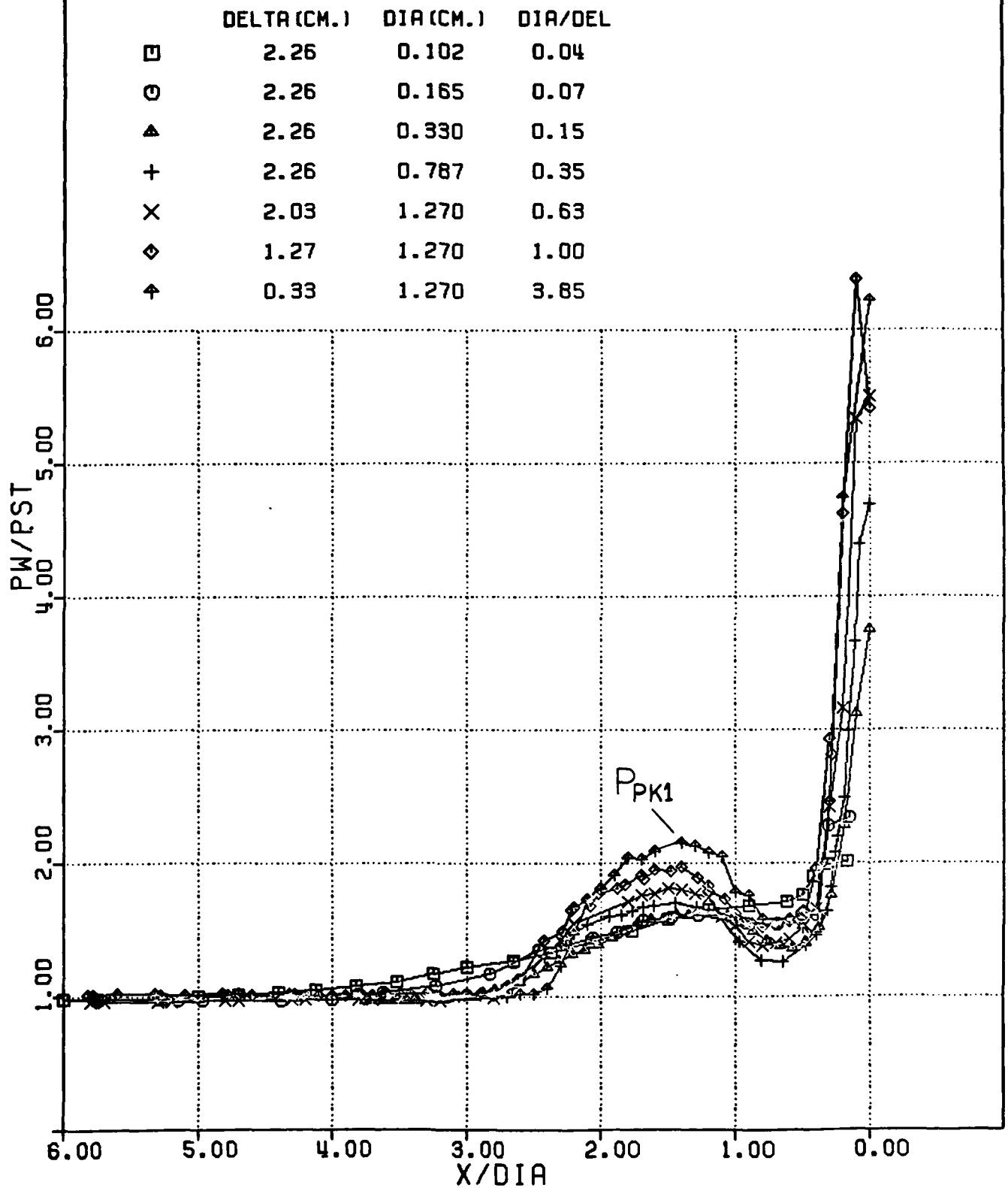


Figure 5. Effect of D/δ on the Plane of Symmetry Pressure Distribution

PLANE OF SYMMETRY PRESSURE DISTRIBUTIONS

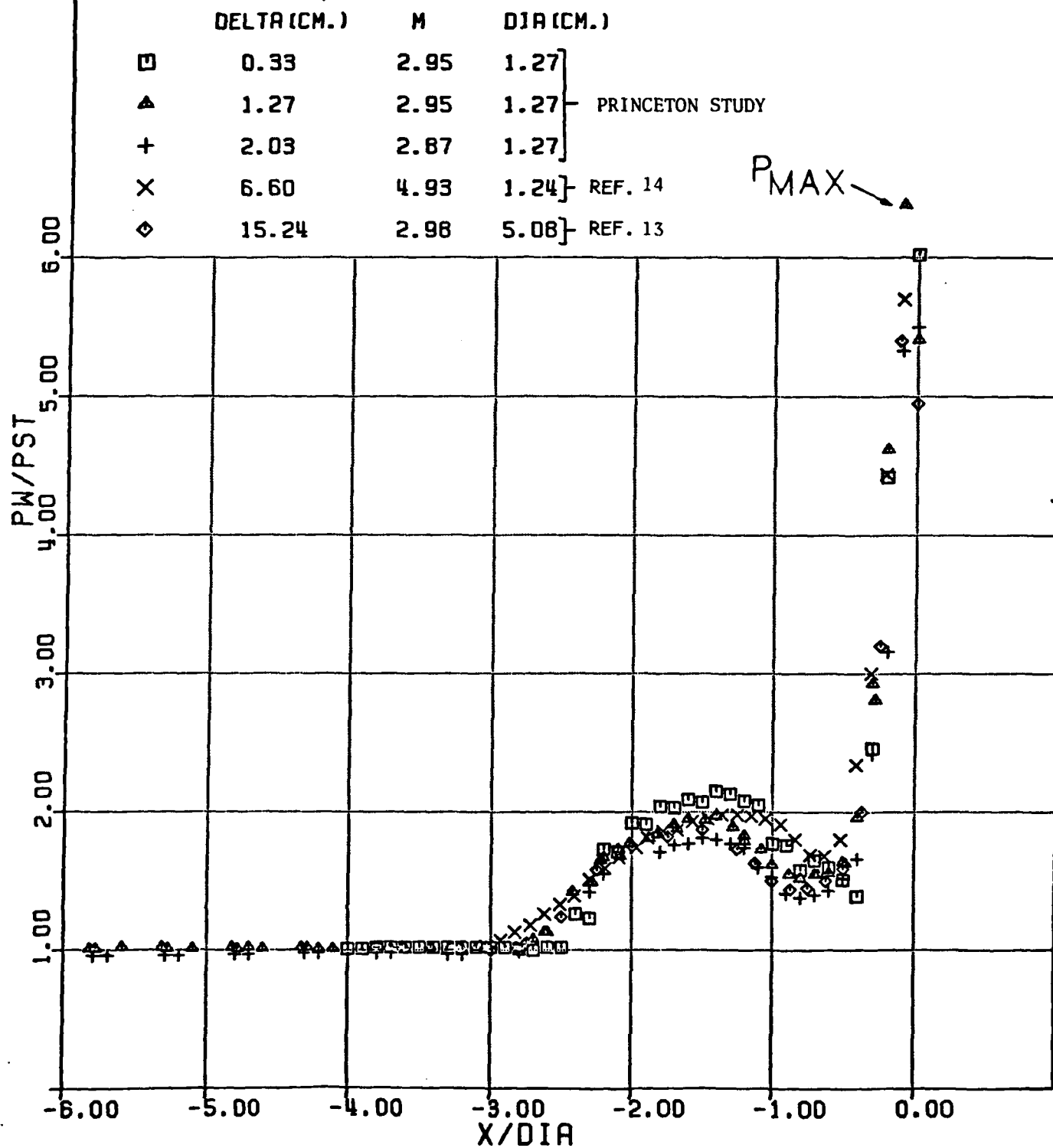


FIGURE 6. Blunt Fin Plane of Symmetry Pressure Distributions.

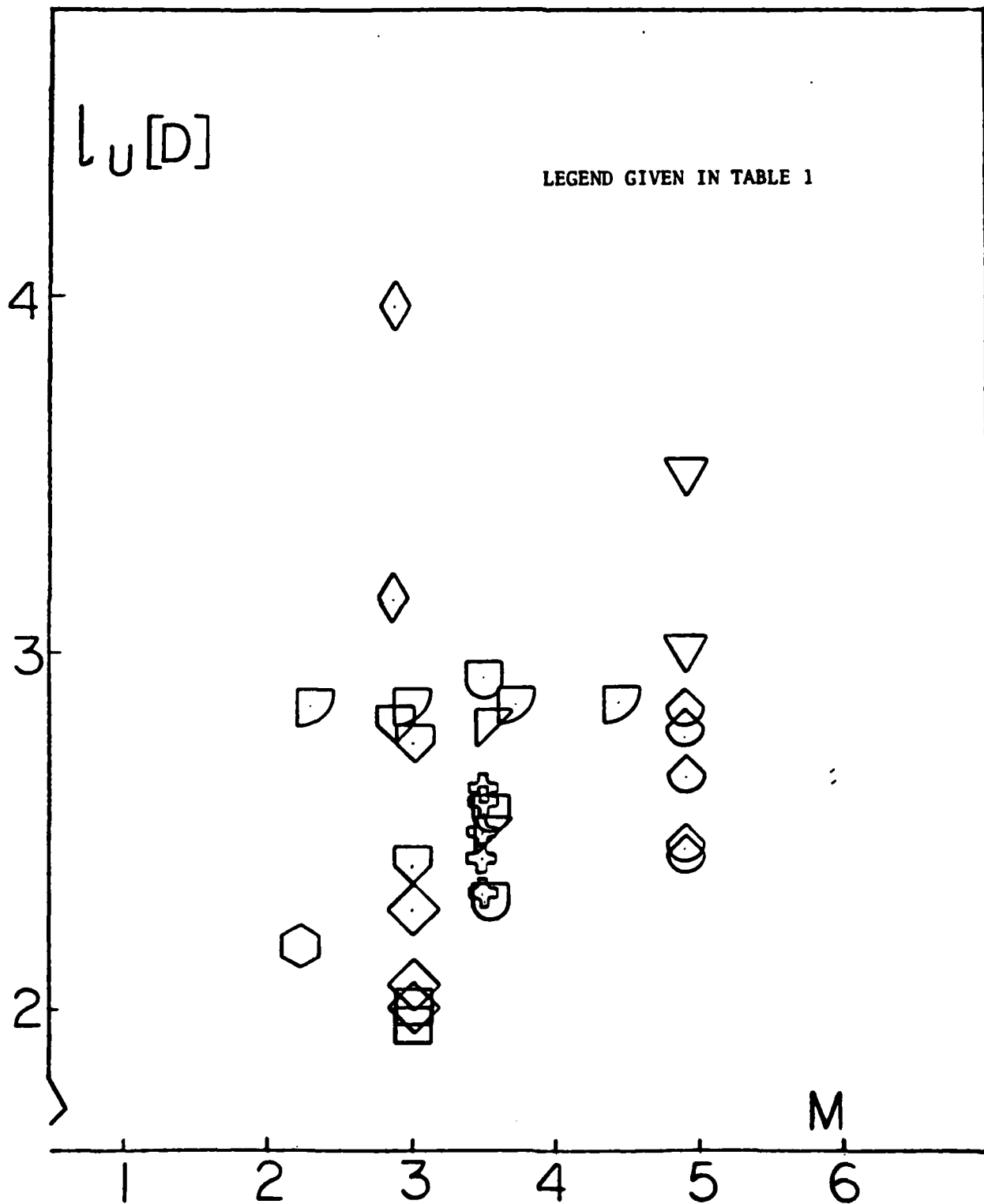


Figure 7. Upstream Influence on the Plane of Symmetry as a Function of Mach Number.

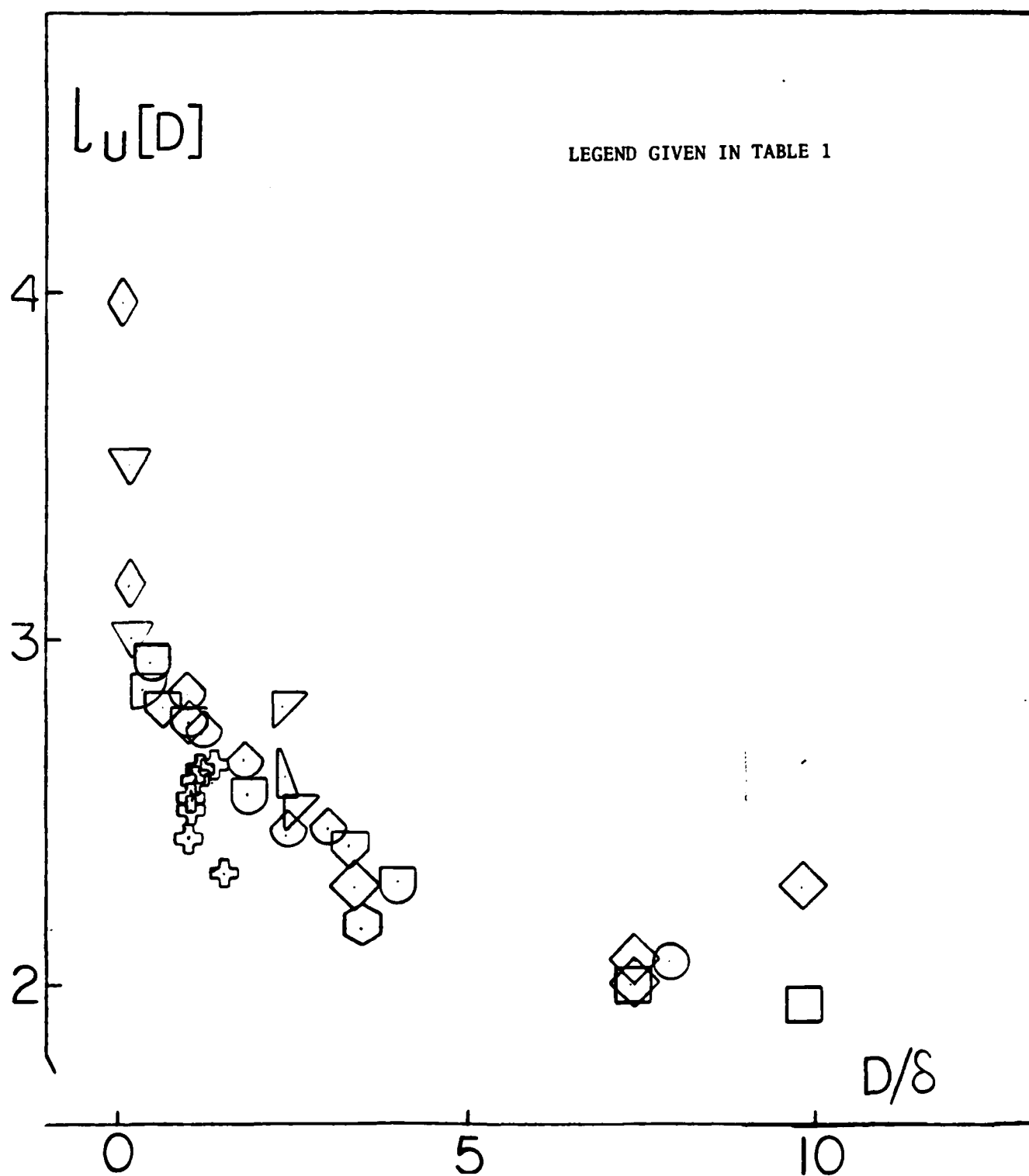


Figure 8. Upstream Influence on the Plane of Symmetry as a Function of D/δ .

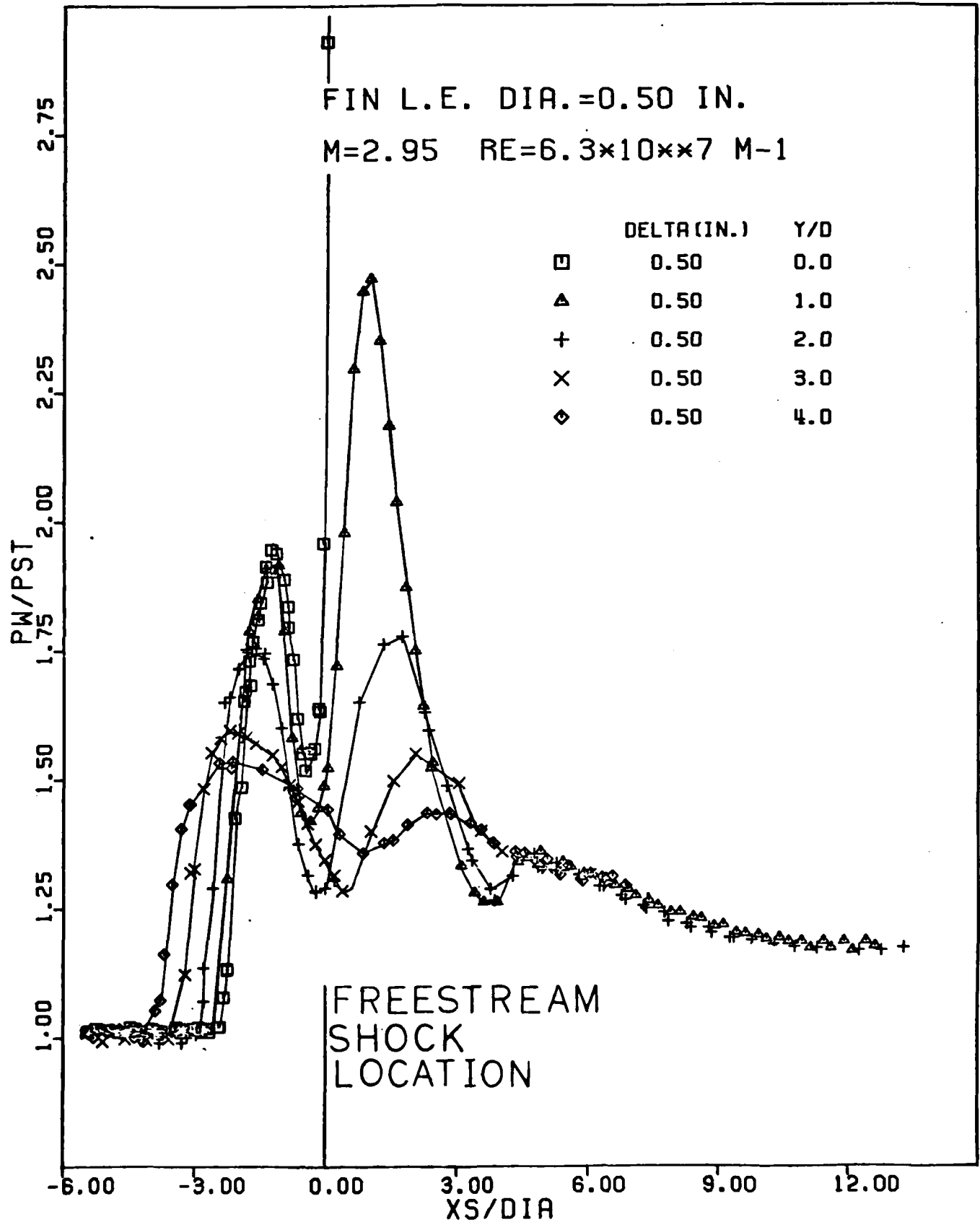


Figure 9. Streamwise Pressure Distributions for $0 \leq Y/D \leq 4.0$

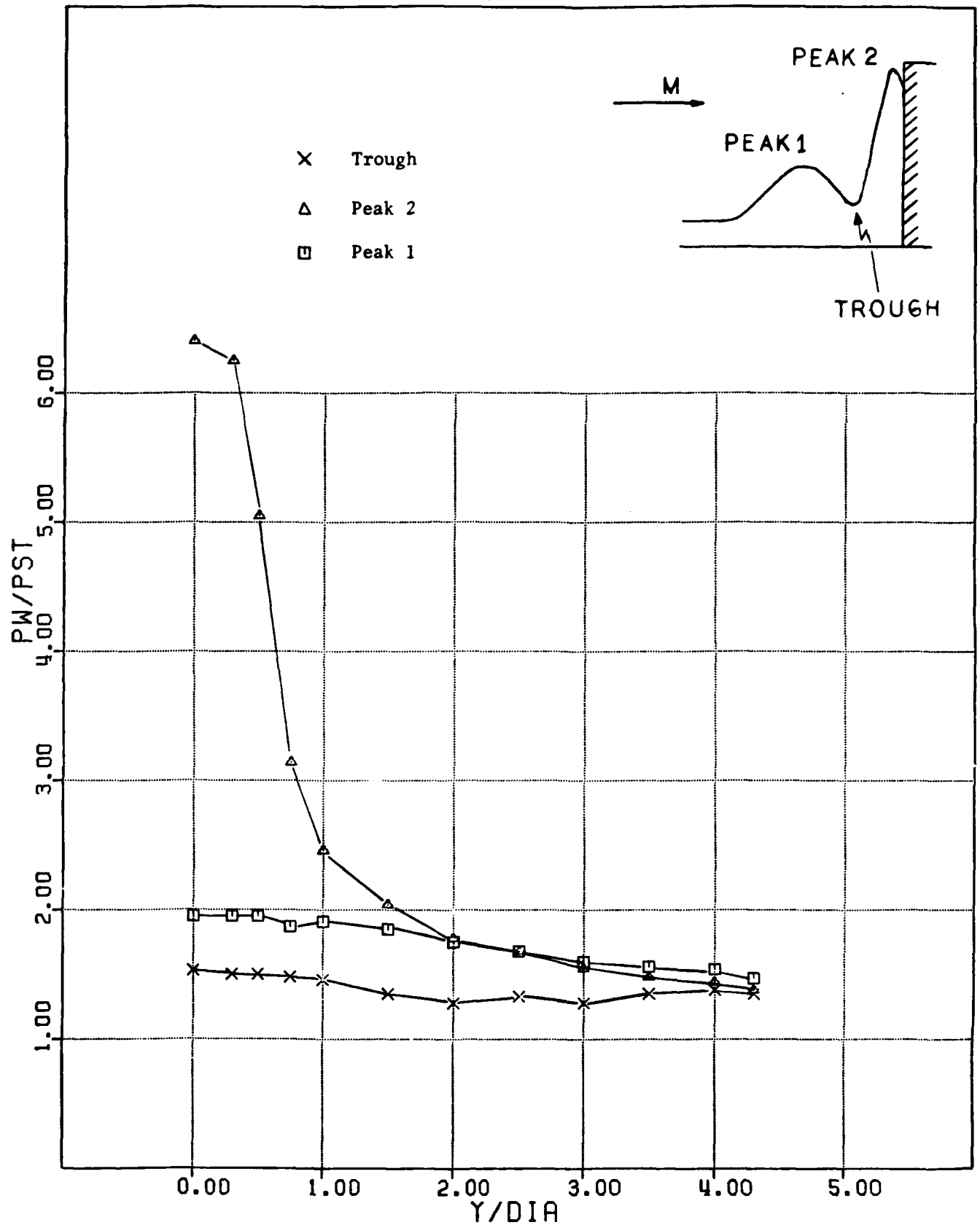


Figure 10. Variation of Peak and Trough Pressures with Y/D

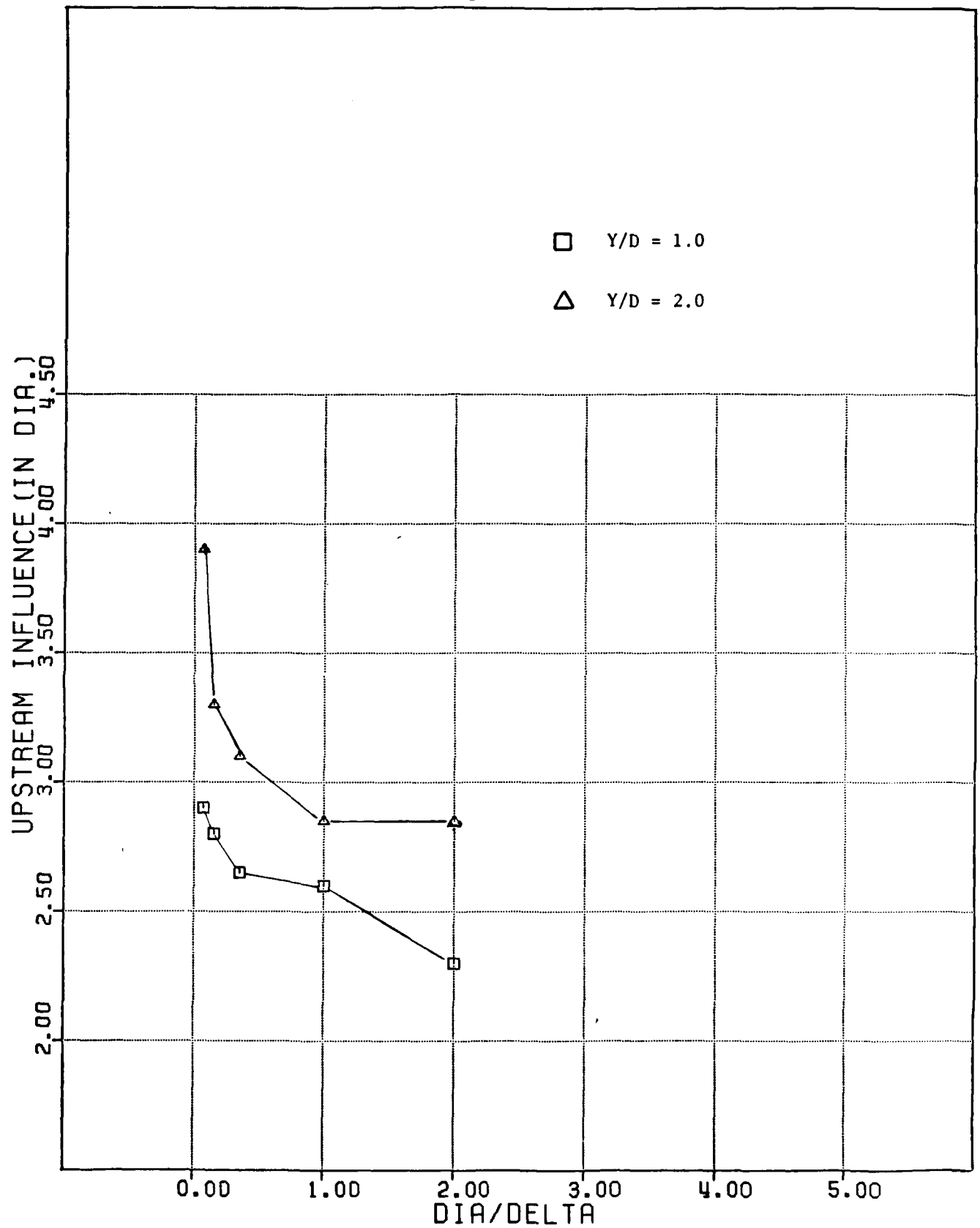


Figure 11. Upstream Influence as a Function of D/δ at $Y/D = 1$ and 2

20/MARCH/1980

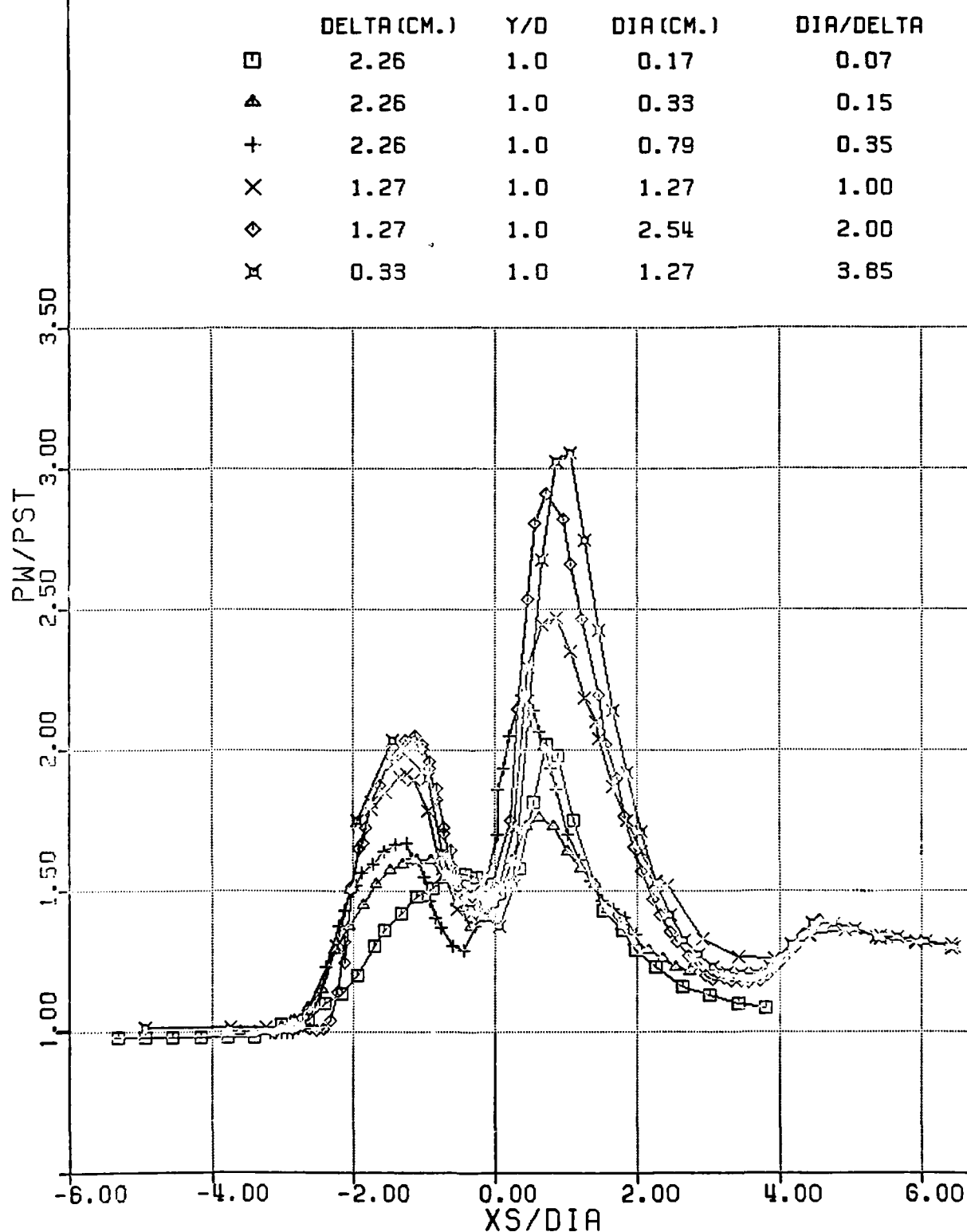


Figure 12. Influence of D/δ on Streamwise Pressure Distributions at $Y/D = 1$

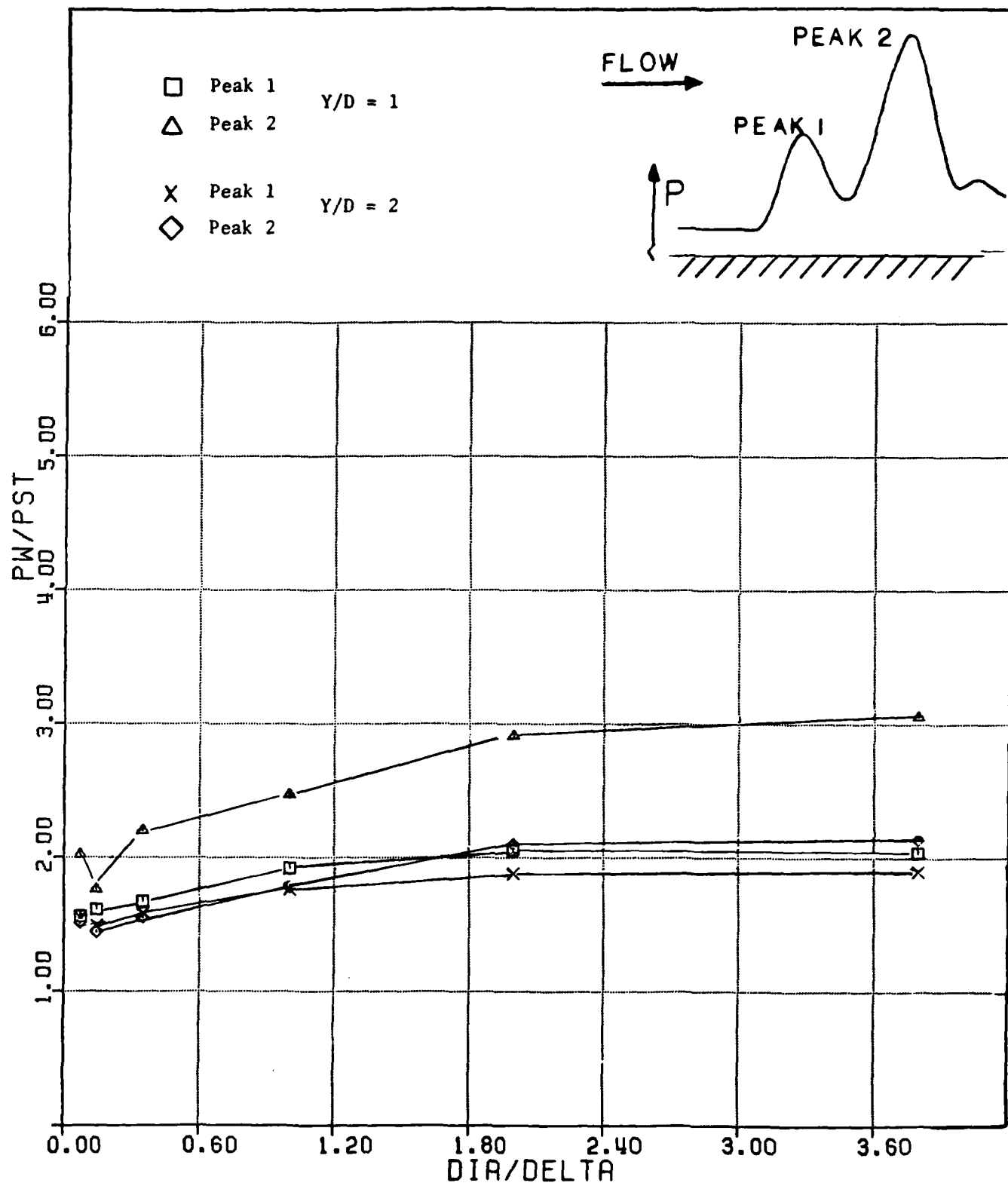


Figure 13. Influence of D/δ on Peak Pressure Levels

19/MARCH/1980

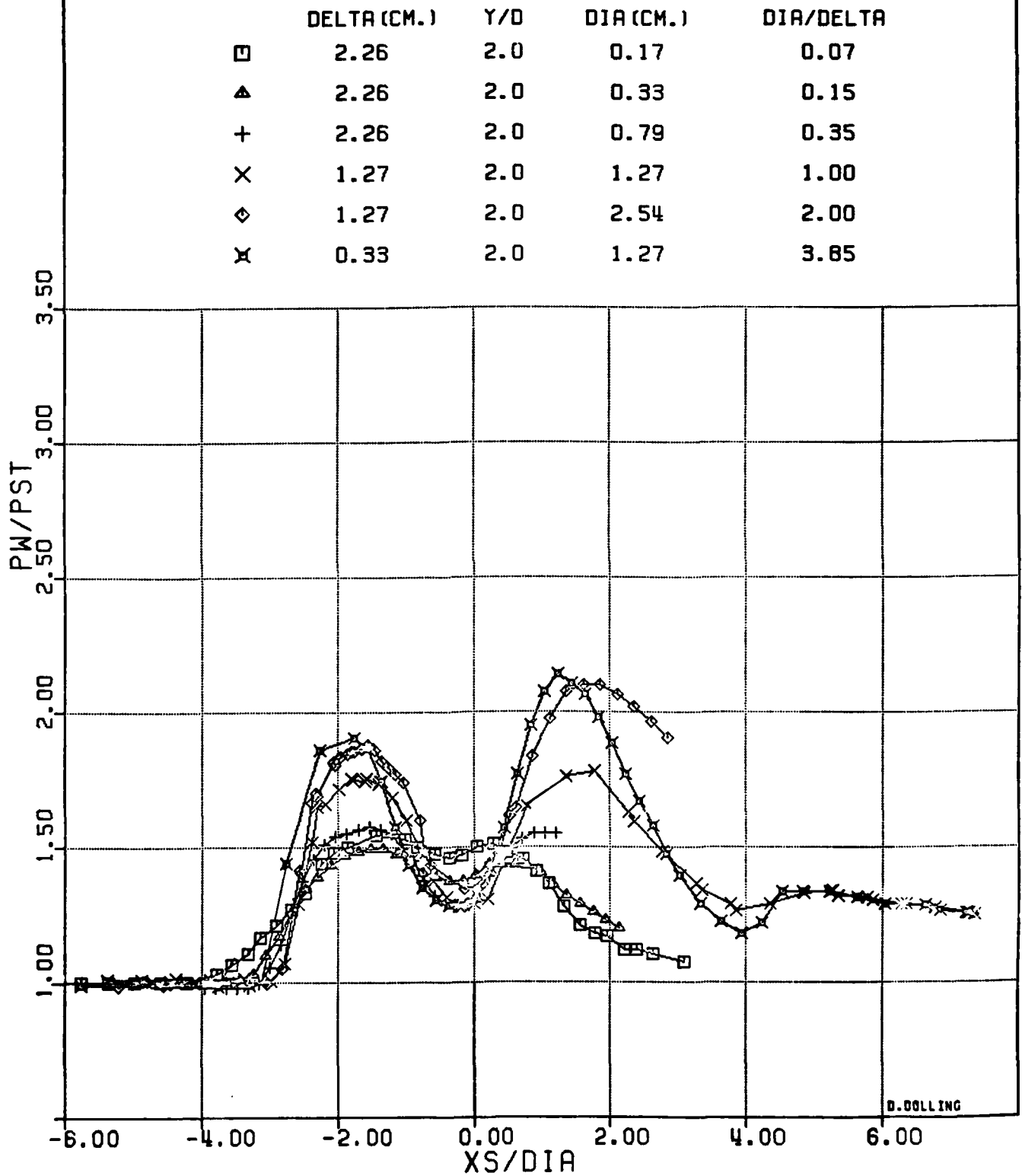


Figure 14. Influence of D/δ on Streamwise Pressure Distributions at $Y/D = 2$

28/03/80

FIN PRESSURE DISTRIBUTIONS

FIN L.E. DIA.=1.27 CM.
M=2.95 RE=6.3×10××7 M-1

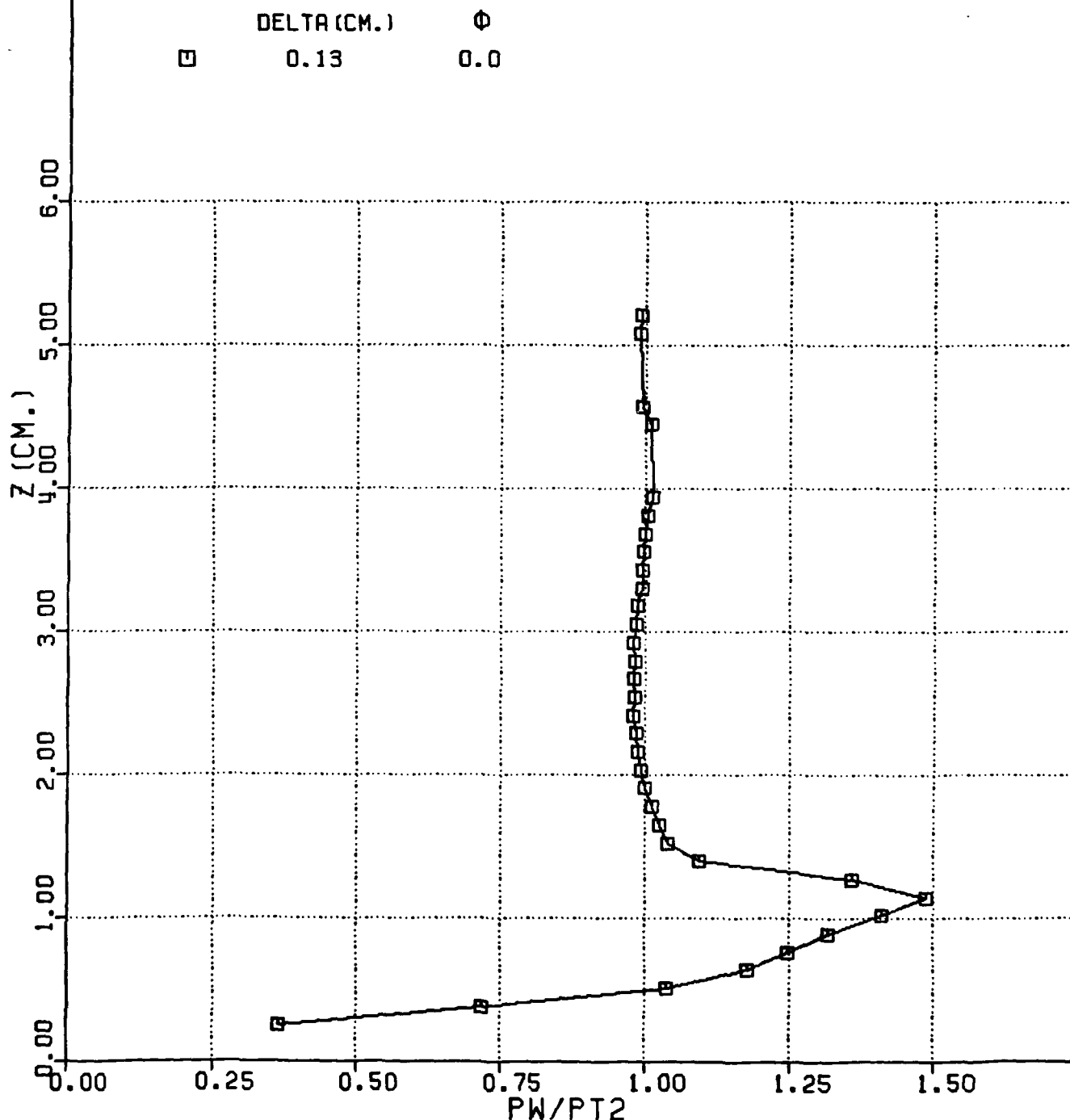


Figure 15. Typical Fin Leading Edge Pressure Distribution

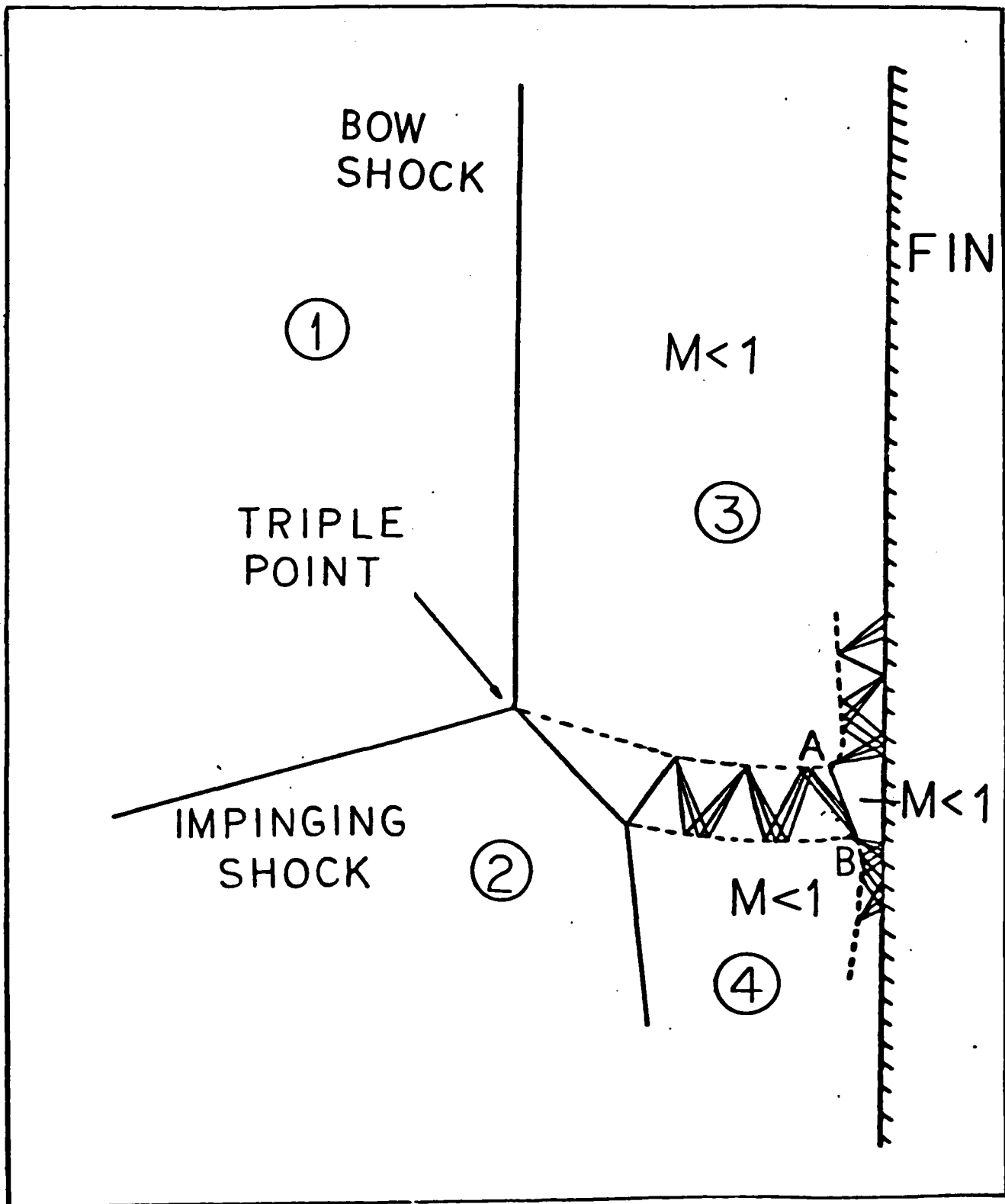


Figure 16. Schematic of Fin Leading Edge Shock Wave Structure

28/03/80

FIN PRESSURE DISTRIBUTIONS

FIN L.E. DIA.=1.27 CM.

M=2.95 RE=6.3×10××7 M-1

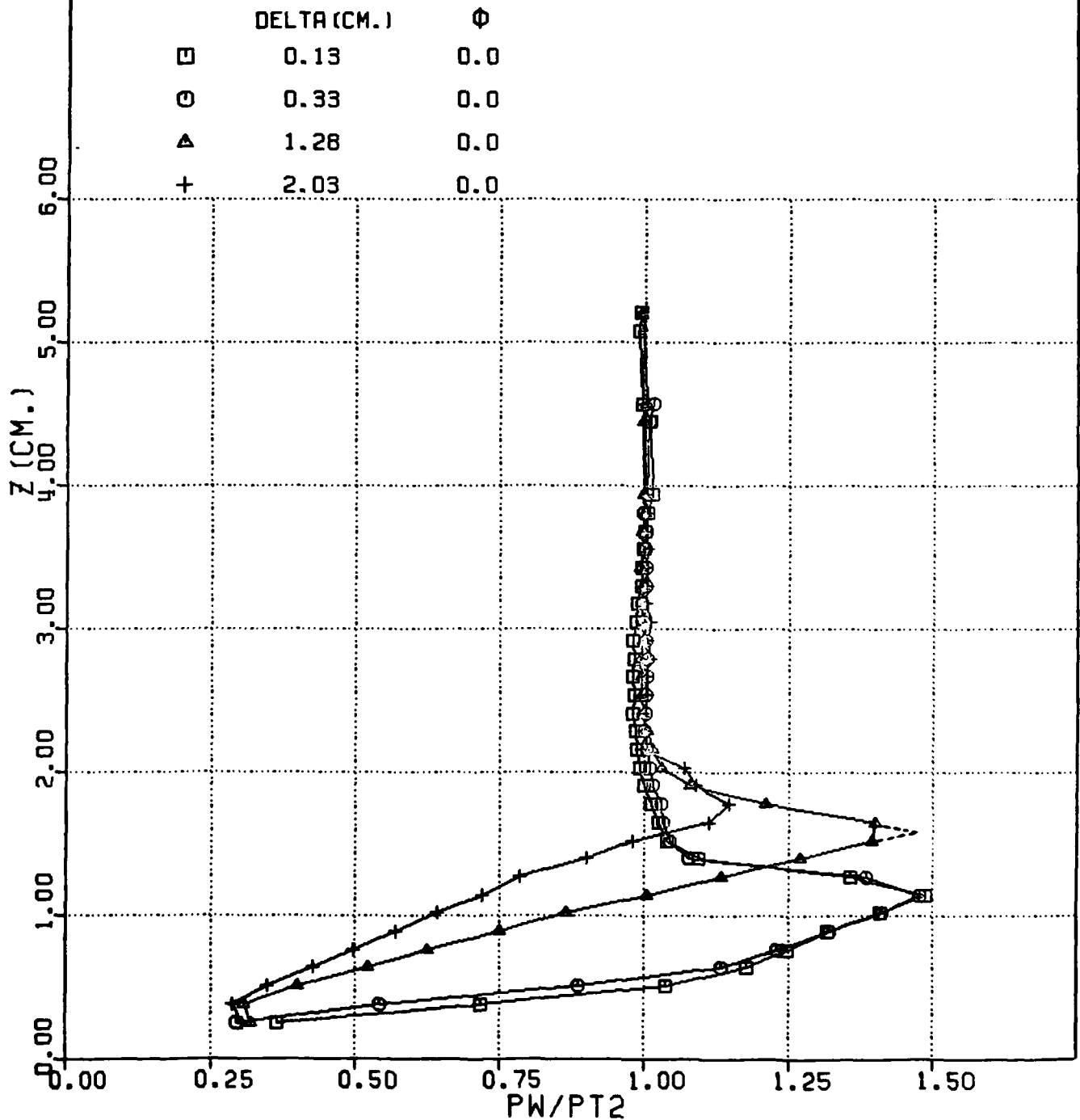


Figure 17. Fin Leading Edge Pressure Distributions for Different Incoming Turbulent Boundary Layers

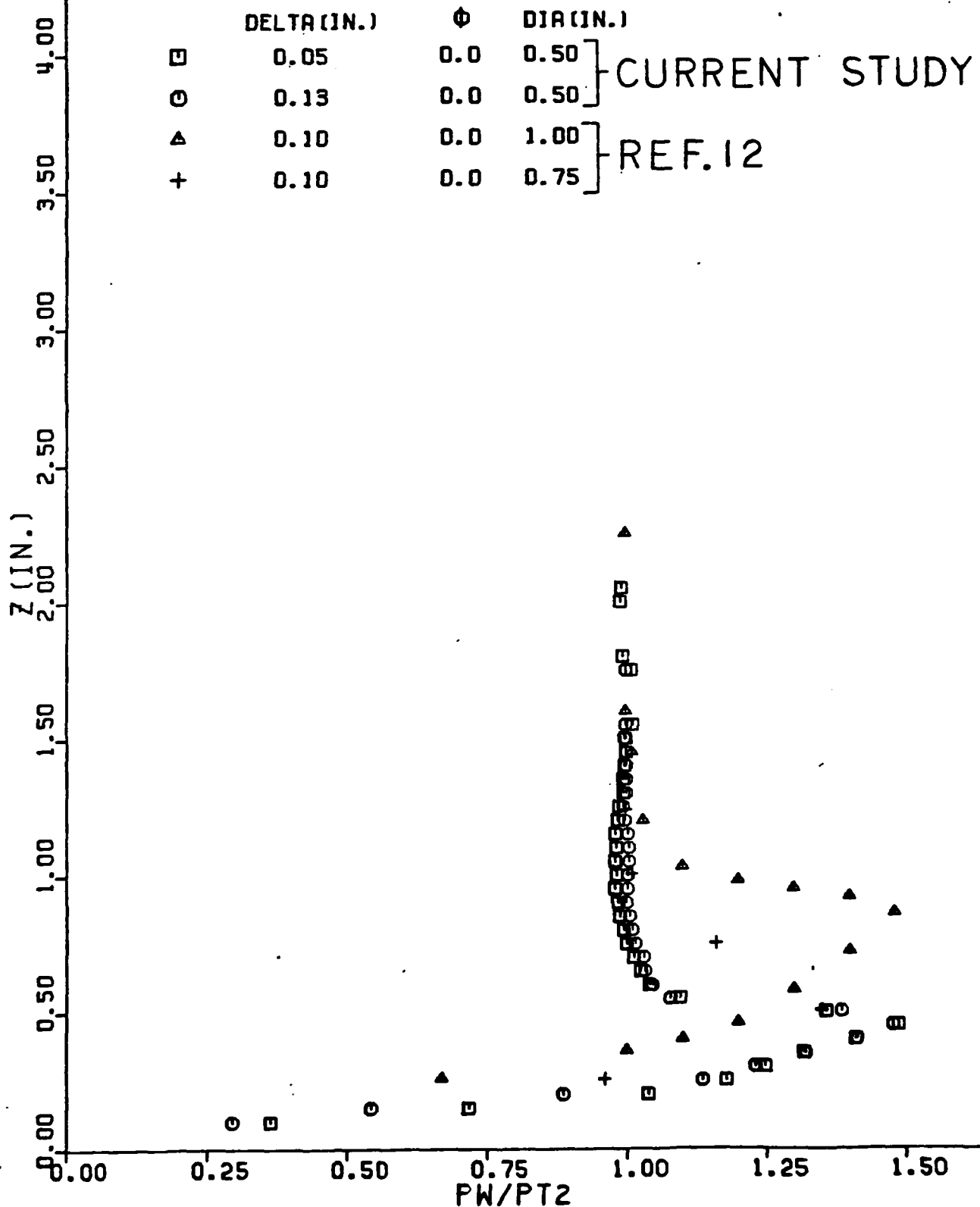


Figure 18. Fin Leading Edge Pressure Distributions from Different Studies Plotted versus Z

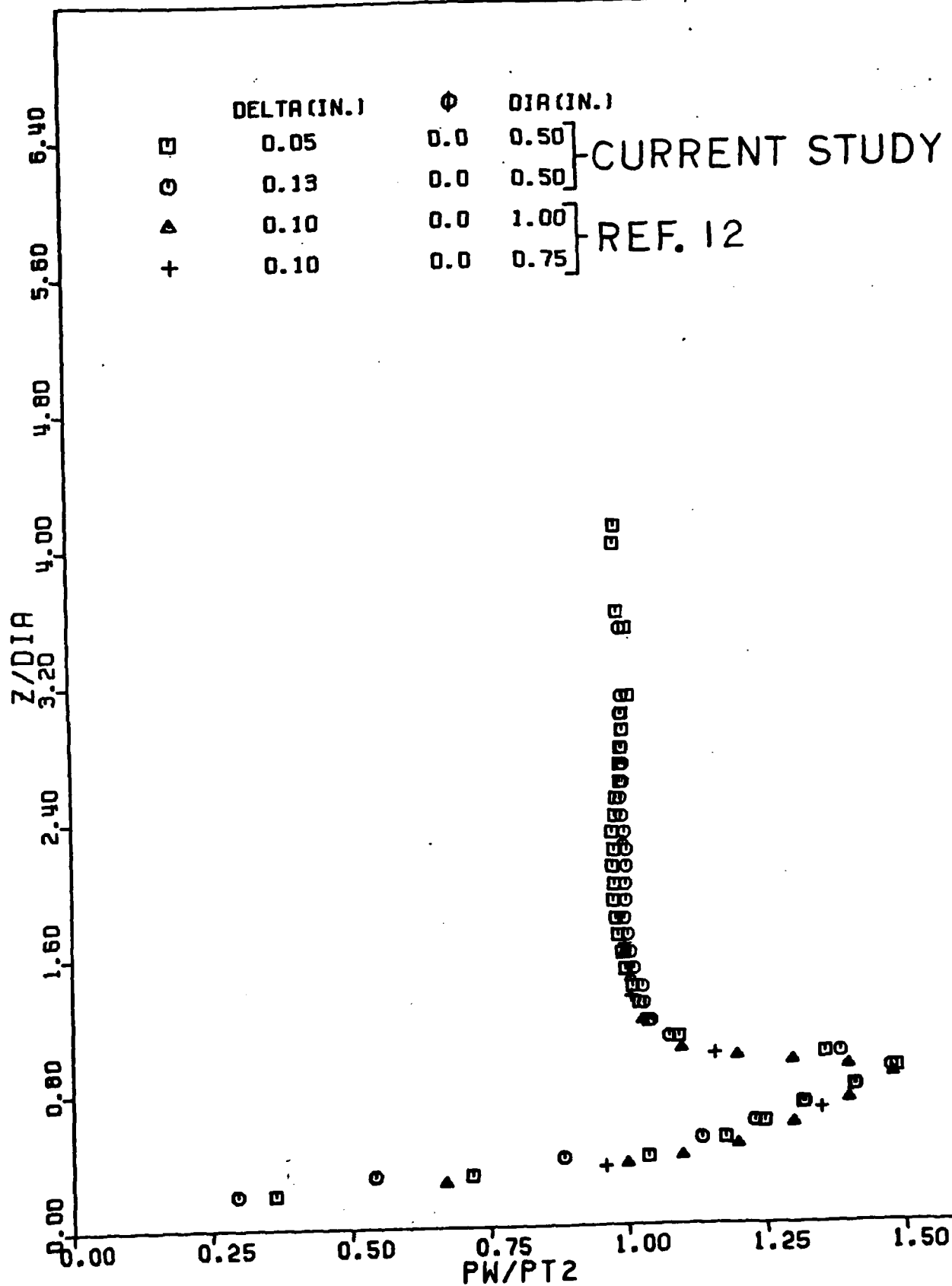


Figure 19. Fin Leading Edge Pressure Distributions from Different Studies
Plotted versus Z/D

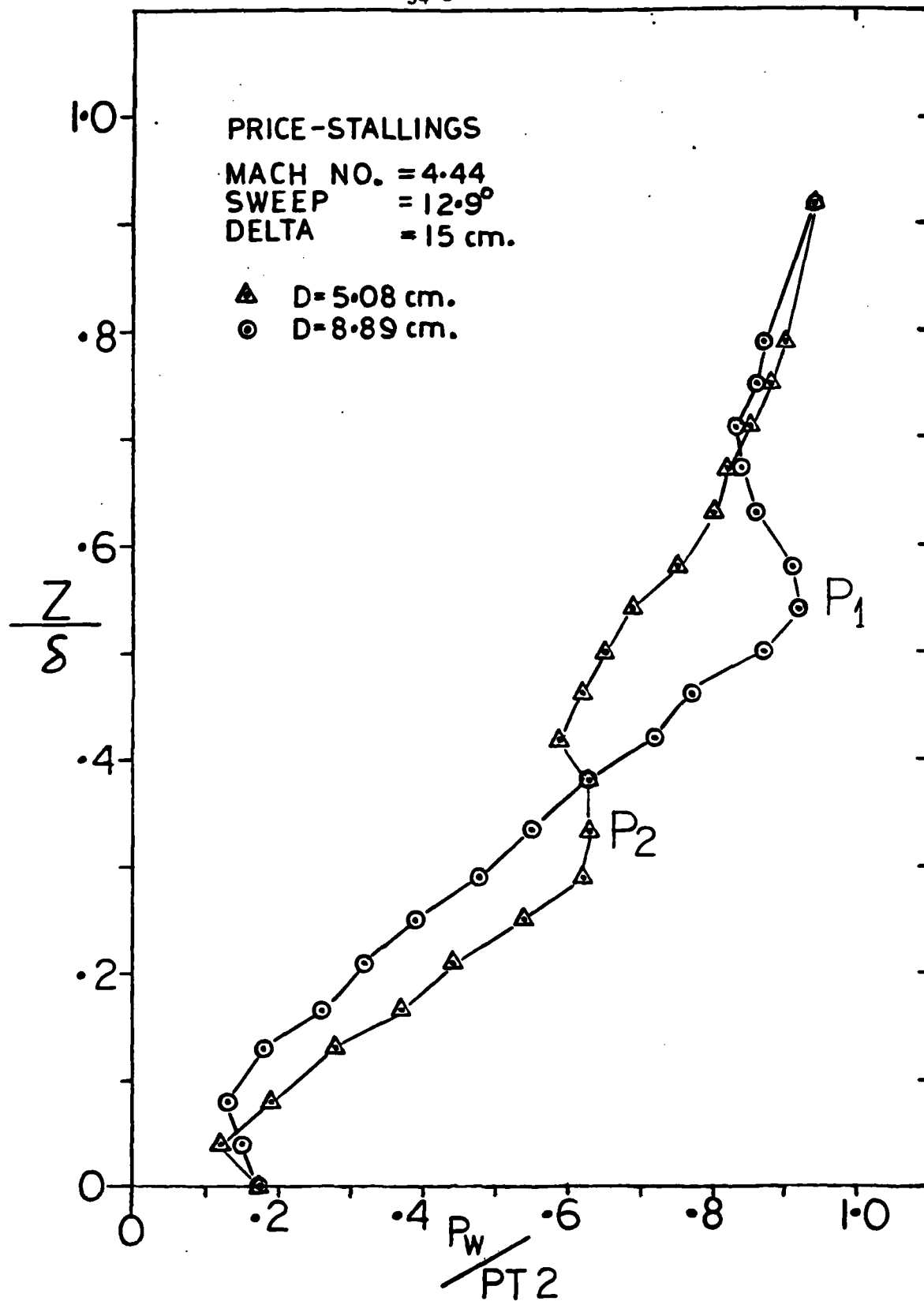


Figure 20. Price and Stalling's Fin Leading Edge Pressure Distributions Plotted versus Z/δ

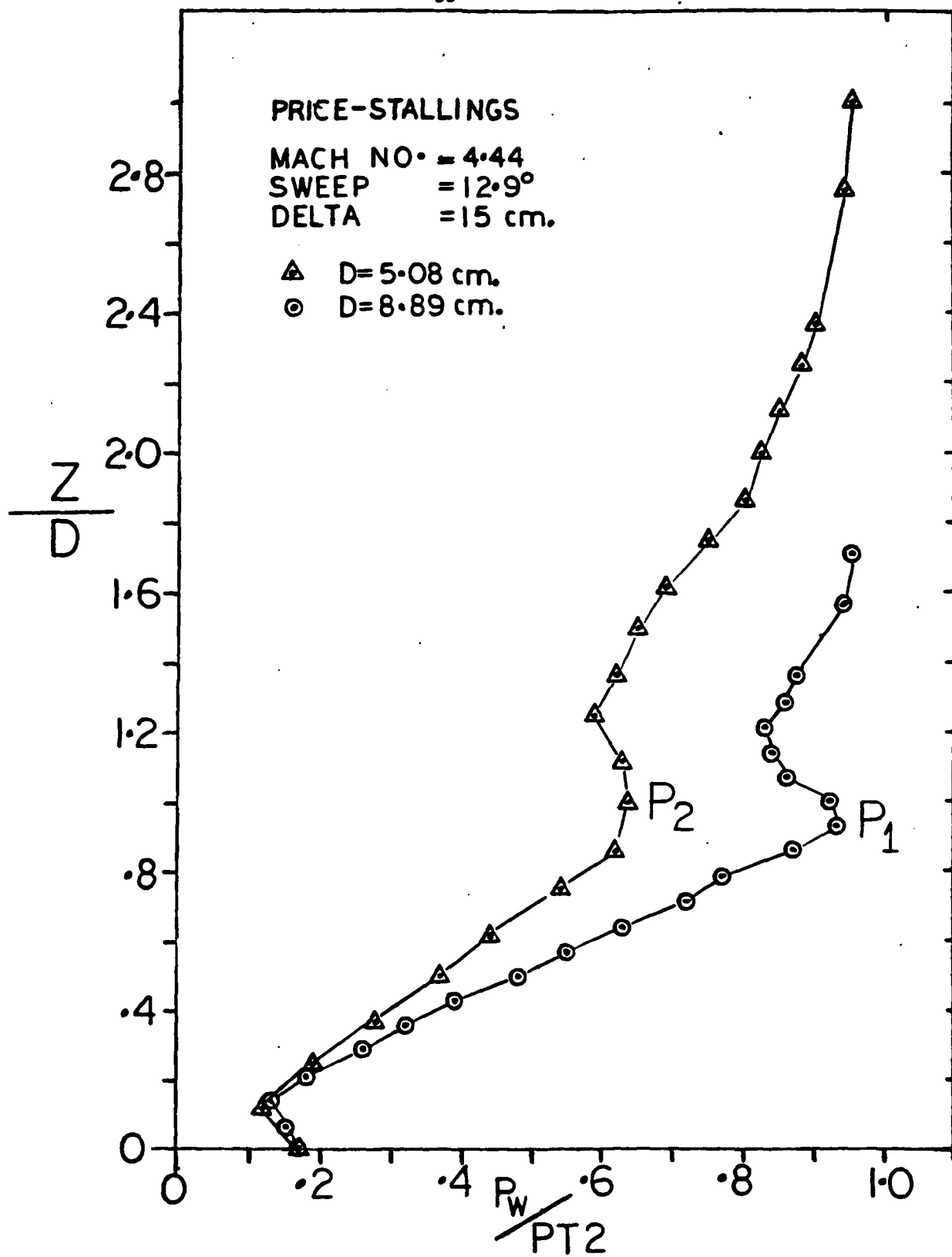


Figure 21. Price and Stalling's Fin Leading Edge Pressure Distributions Plotted versus Z/D

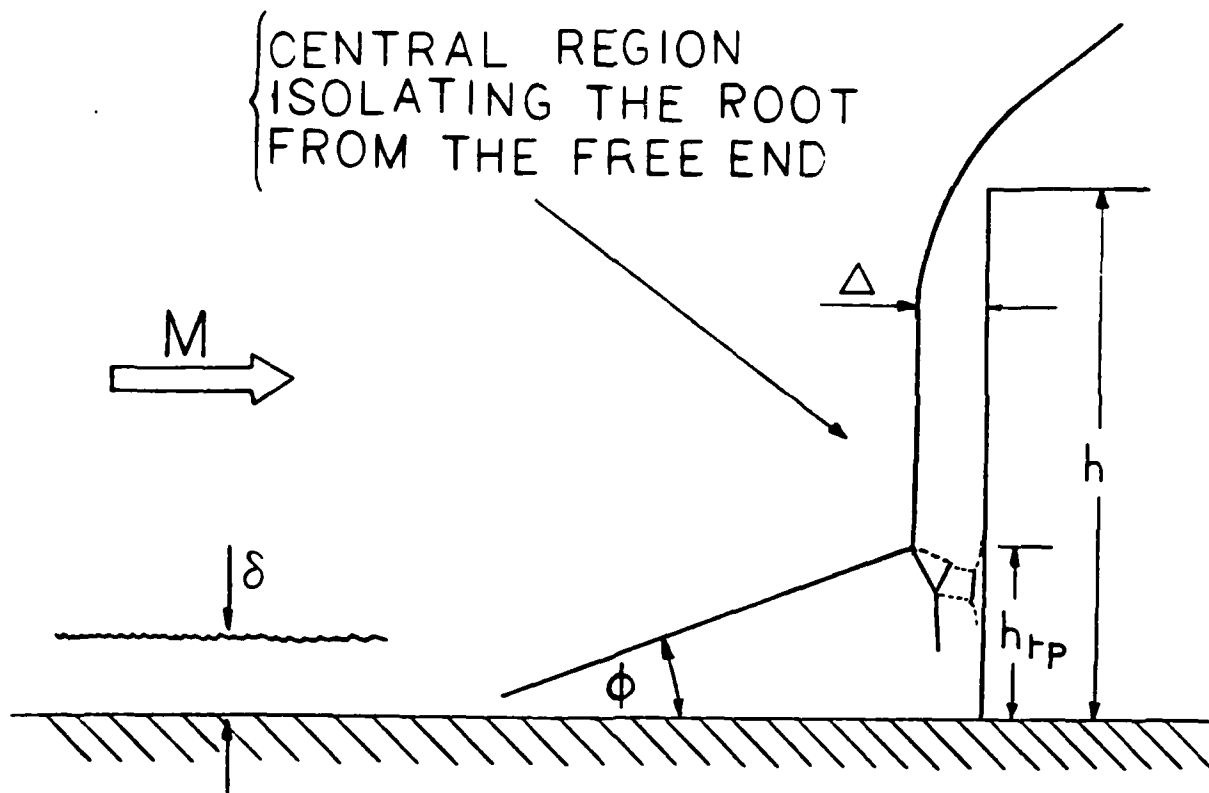


Figure 22. Schematic of Shock Structure Illustrating Fin Height Needed to Generate "asymptotic" Flowfield

12/03/80

FIN PRESSURE DISTRIBUTIONS

FIN L.E. DIA.=1.27 CM.

M=2.95 RE=6.3×10××7 M-1

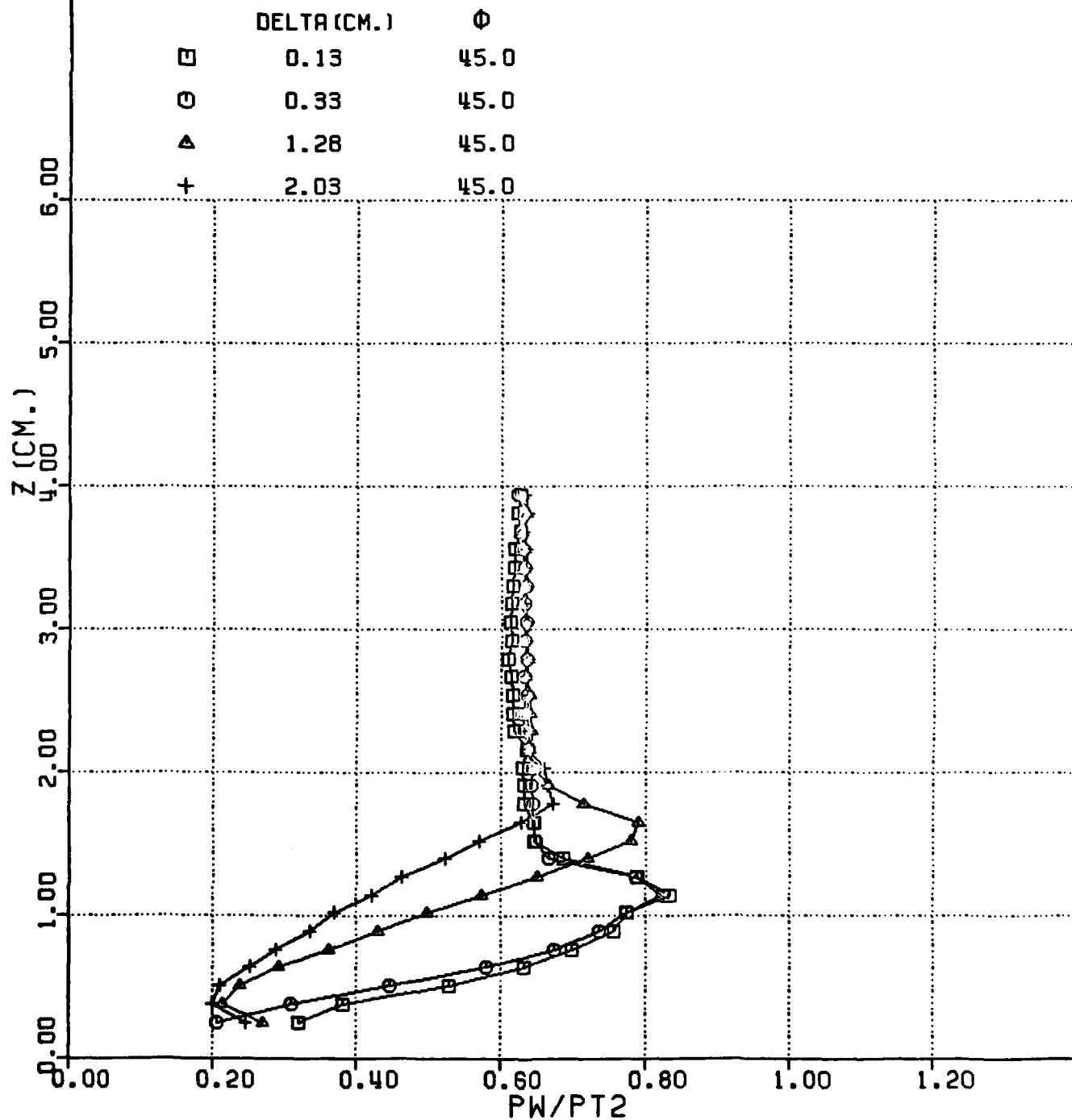


Figure 23. Fin Leading Edge ($\phi = 45^\circ$) Pressure Distributions for Different Turbulent Boundary Layers

12/03/80

FIN PRESSURE DISTRIBUTIONS

FIN L.E. DIA.=1.27 CM.

M=2.95 RE=6.3×10××7 M-1

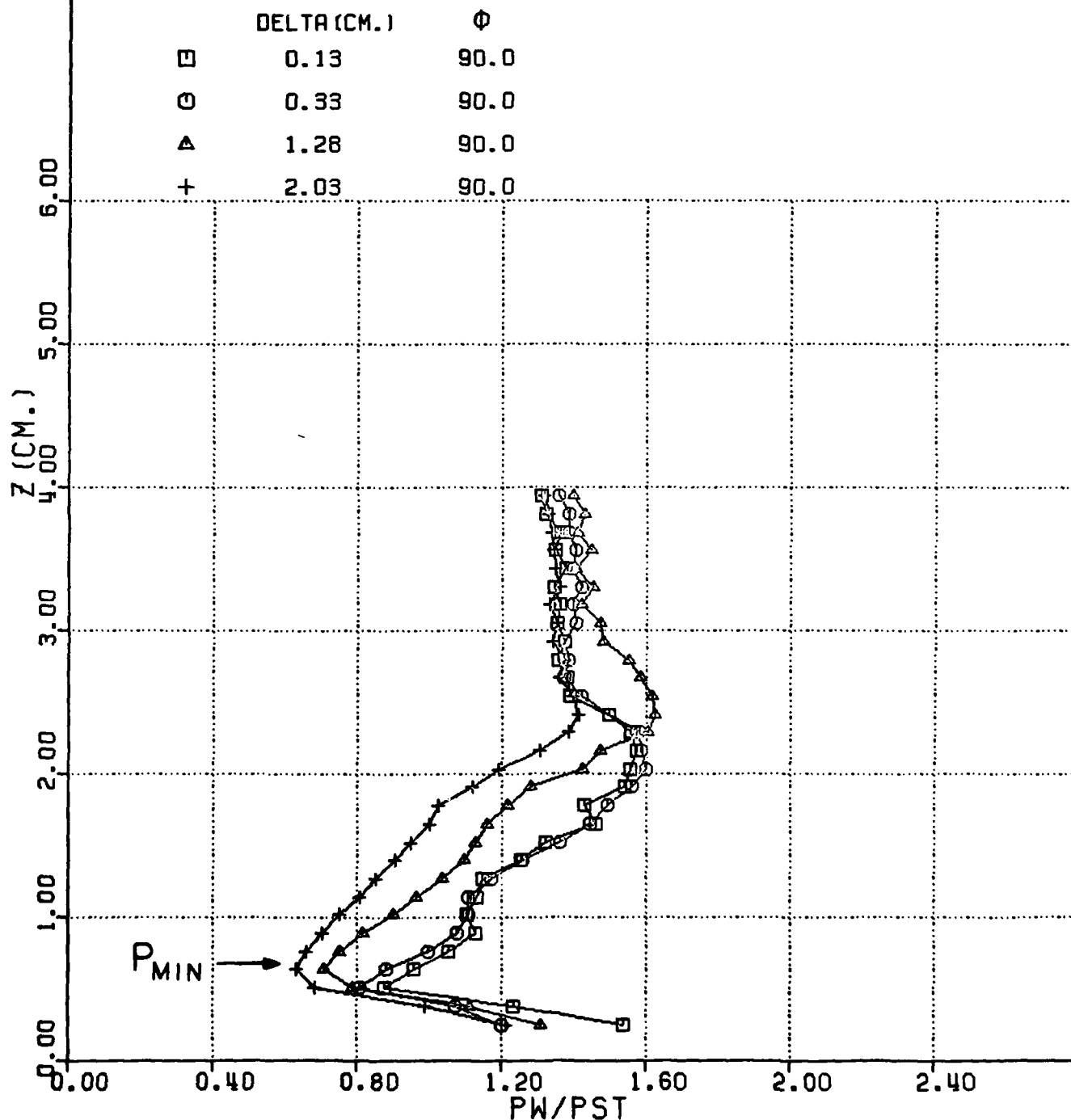


Figure 24. Pressure Distributions at Fin Leading Edge/Body Junction
(i.e., $\phi = 90^\circ$)

13/03/80

FIN PRESSURE DISTRIBUTIONS

FIN L.E. DIA.=1.27 CM.

M=2.95 RE=6.3×10××7 M-1

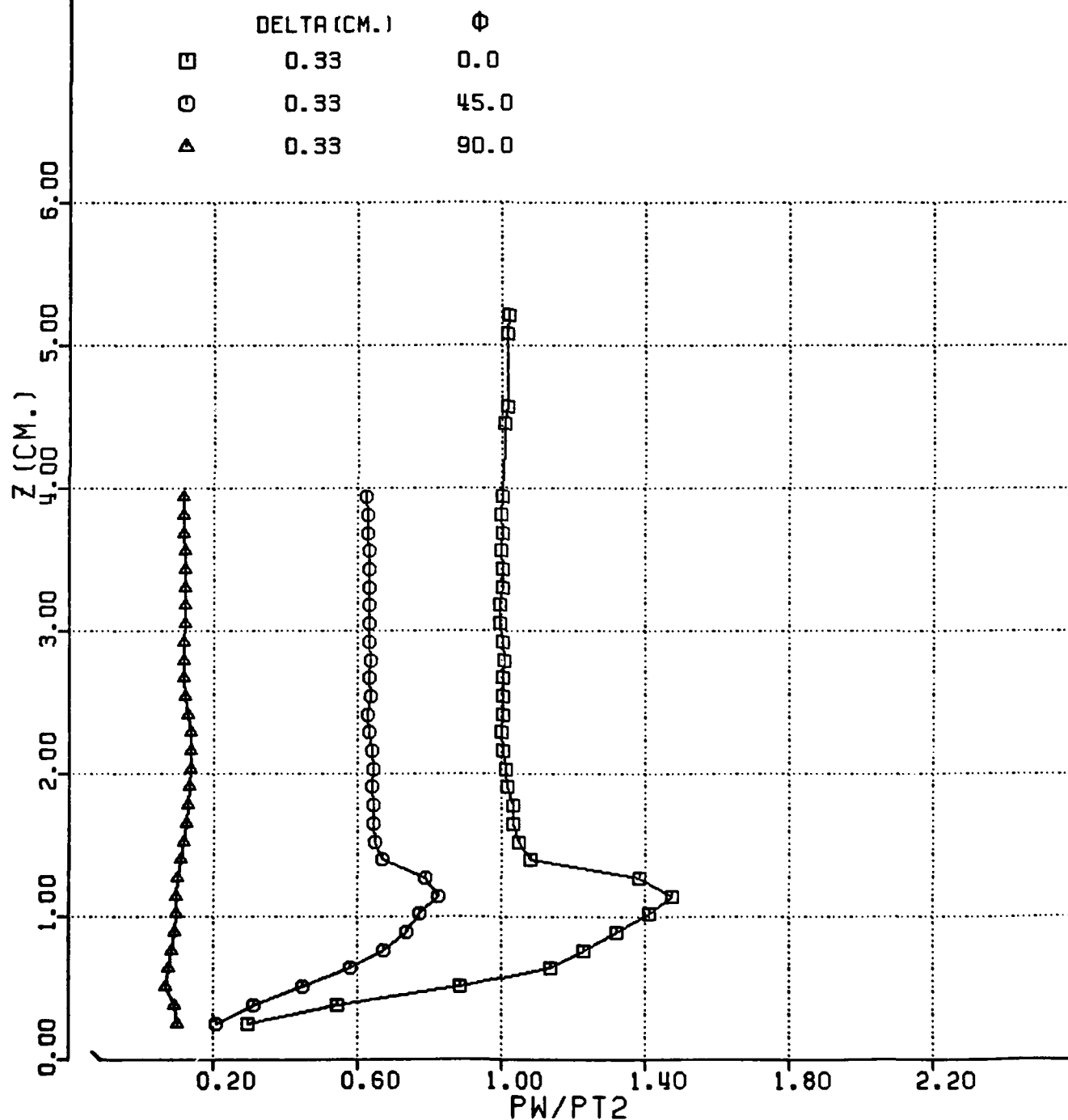


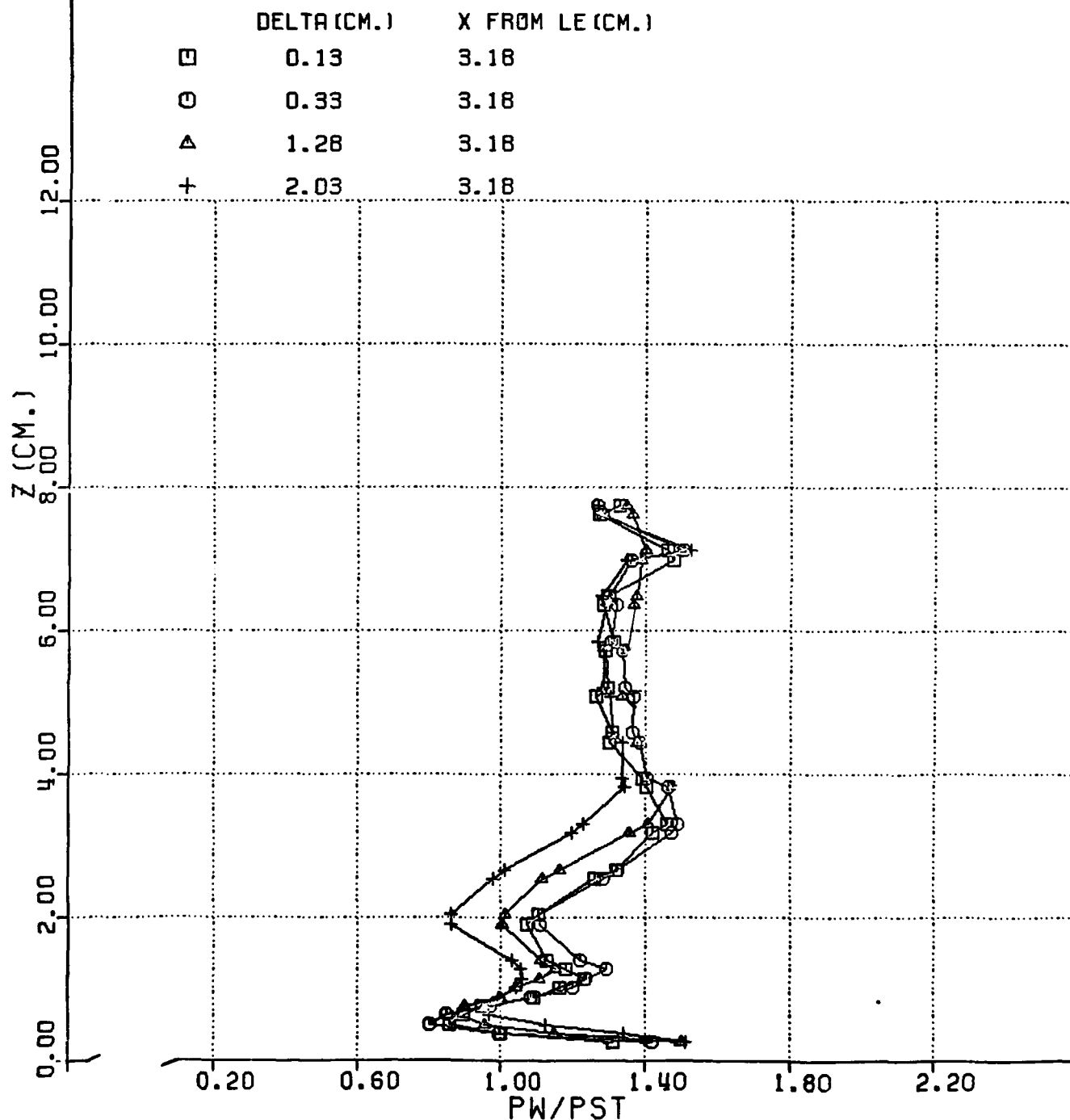
Figure 25. Fin Leading Edge Pressure Distributions at $\phi = 0^\circ, 45^\circ$ and 90°

31/03/80

FIN PRESSURE DISTRIBUTIONS

FIN L.E. DIA.=1.27 CM.

M=2.95 RE=6.3×10××7 M-1



28/03/80

FIN PRESSURE DISTRIBUTIONS

FIN L.E. DIA.=1.27 CM.
M=2.95 RE=6.3×10××7 M-1

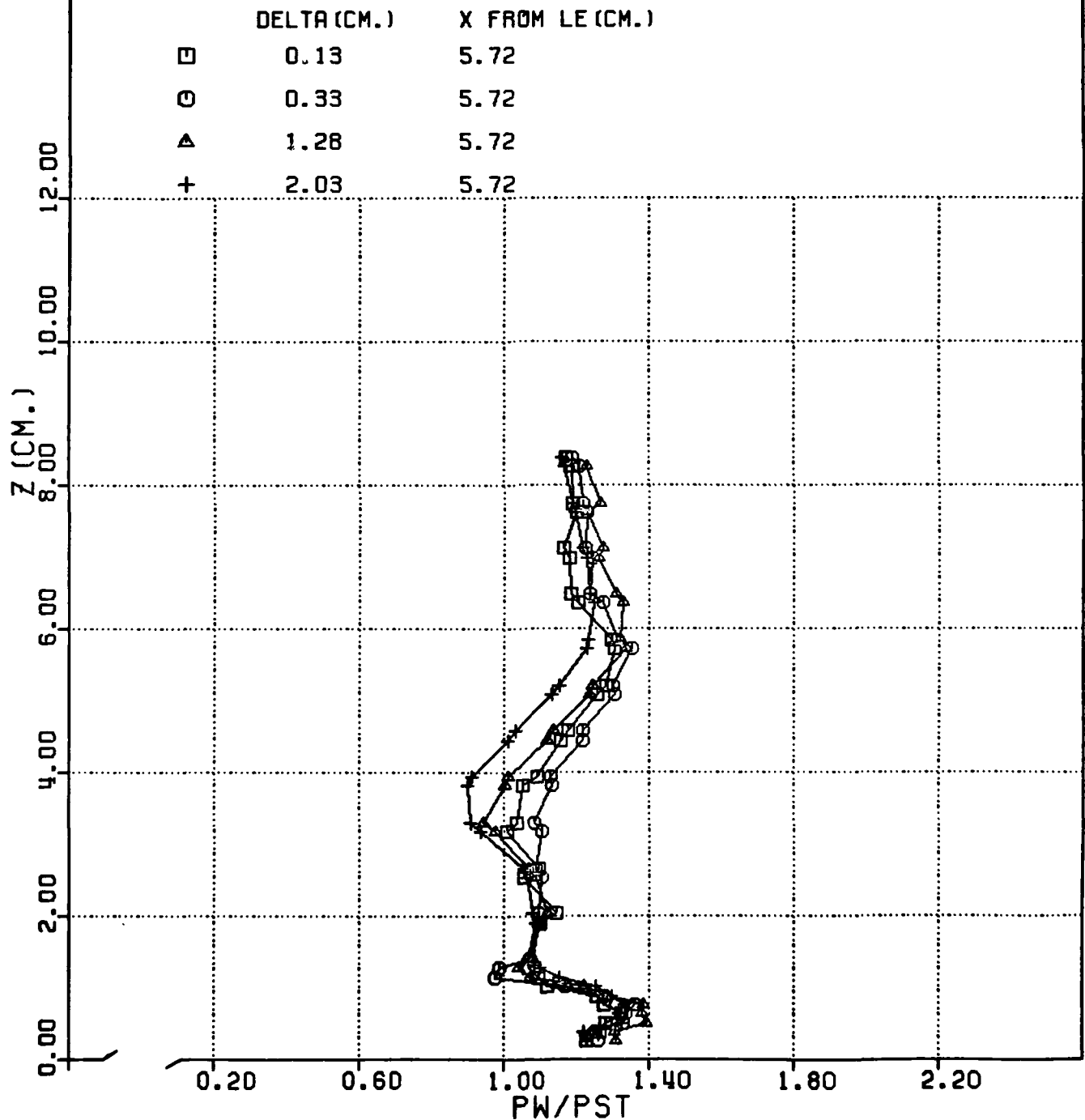


Figure 27. Fin Body Pressure Distributions 5.72 cm from Leading Edge

28/03/80

FIN PRESSURE DISTRIBUTIONS

FIN L.E. DIA.=1.27 CM.

M=2.95 RE=6.3×10××7 M-1

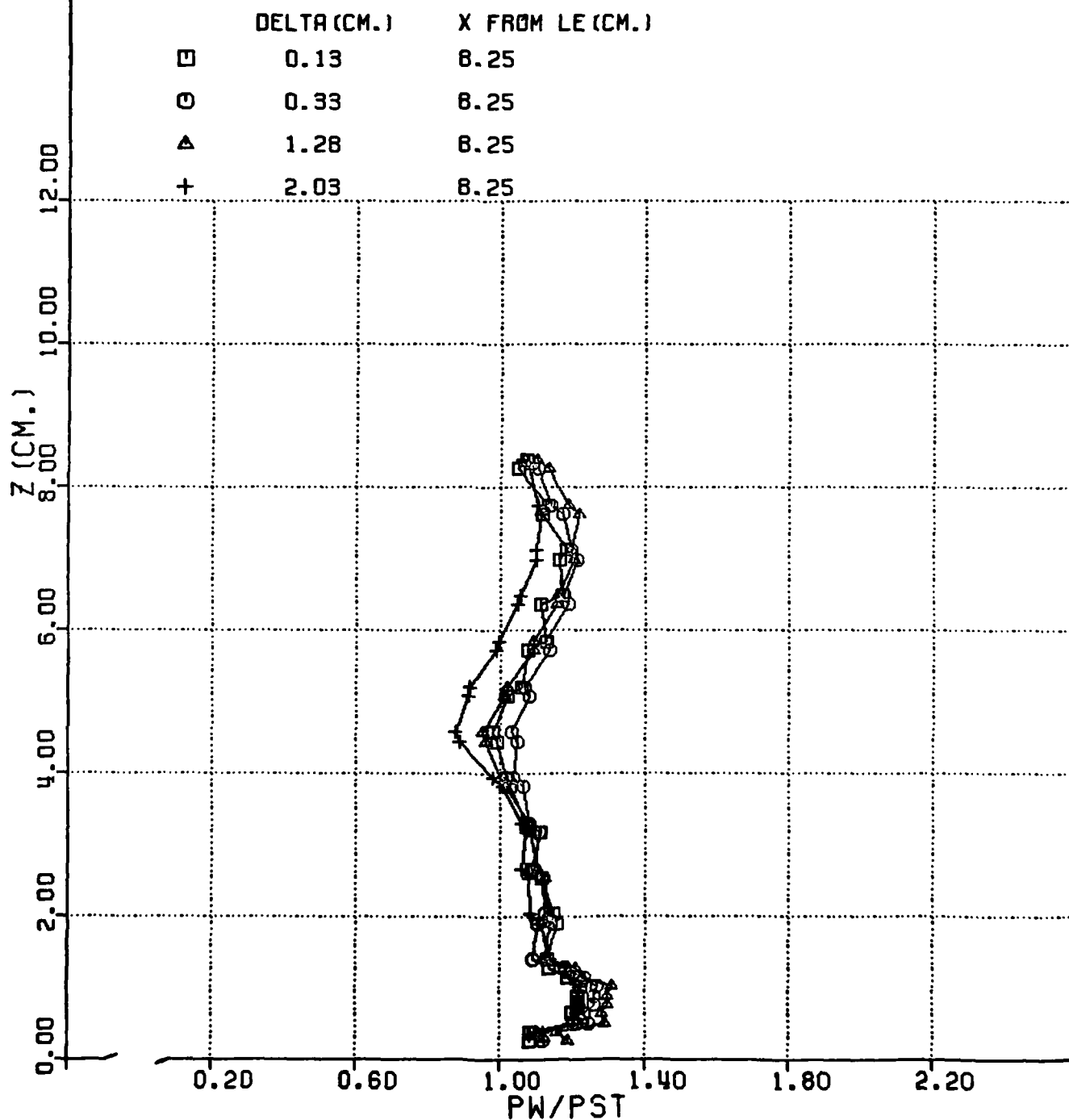


Figure 28. Fin Body Pressure Distributions 8.25 cm from the Leading Edge

14/03/80

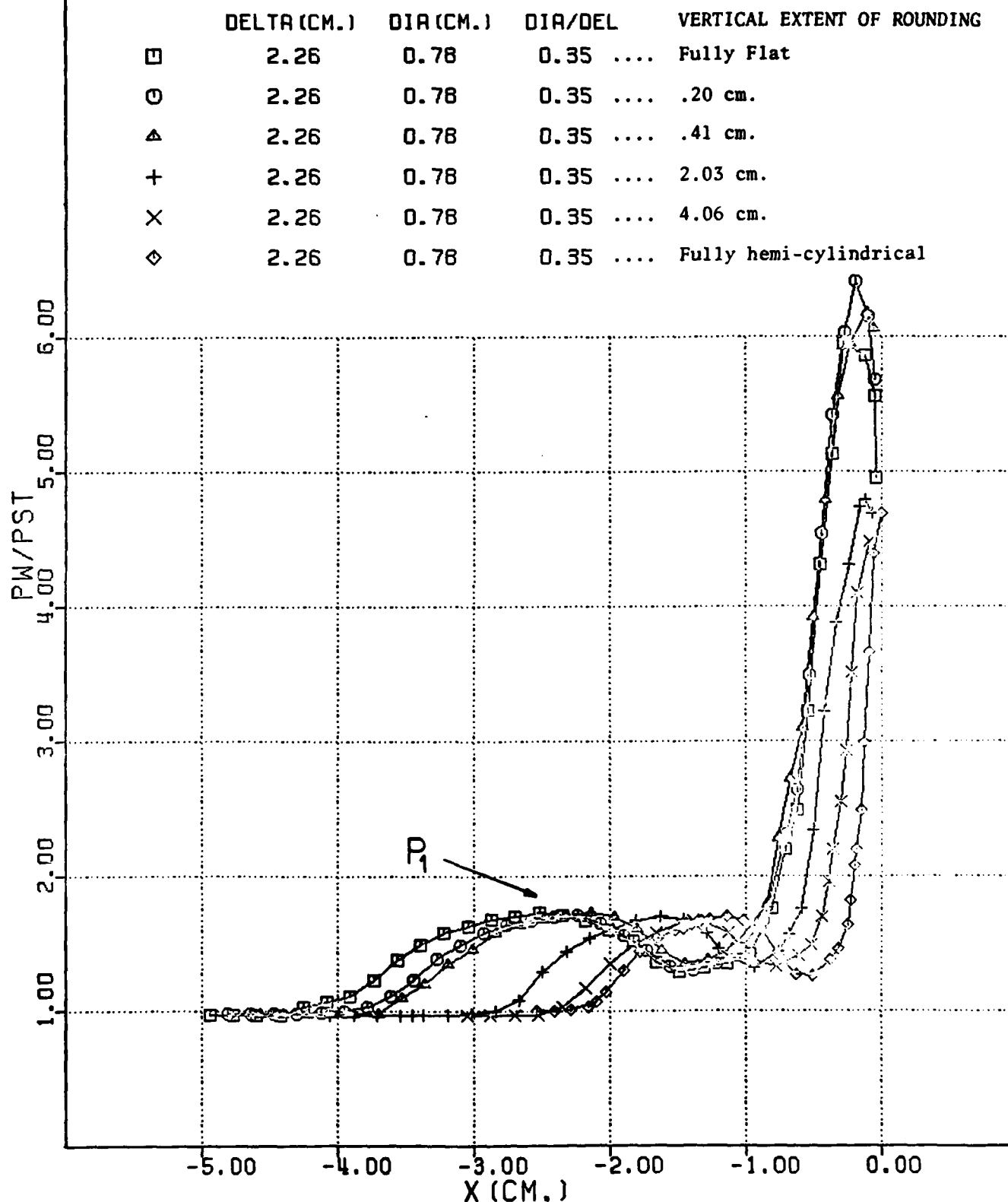
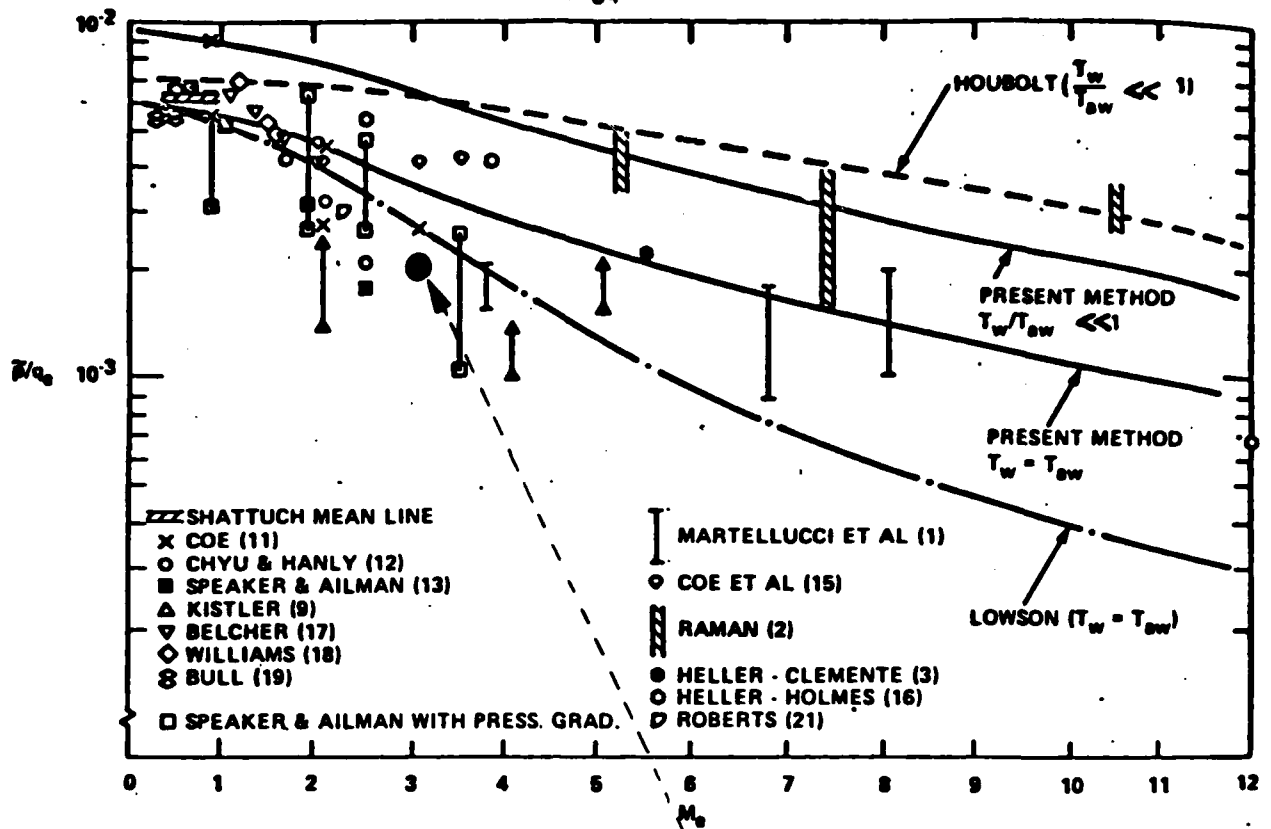
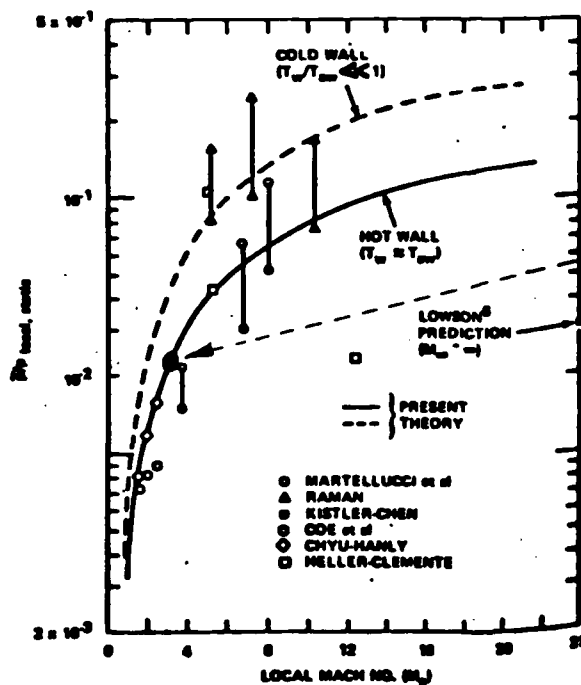


Figure 29. Influence of Leading Edge Geometry on the Plane of Symmetry Pressure Distribution



a) Root Mean Square Pressure Fluctuations Versus Mach Number for Attached Turbulent Flow



b) Pressure Magnitude Normalized with Static Value

Current data

References referred to in these figures are those of Laganelli, et.al.[34]

Figure 30. Surface Pressure Fluctuation Levels in the Undisturbed Turbulent Boundary Layer (figures from Laganelli [34])

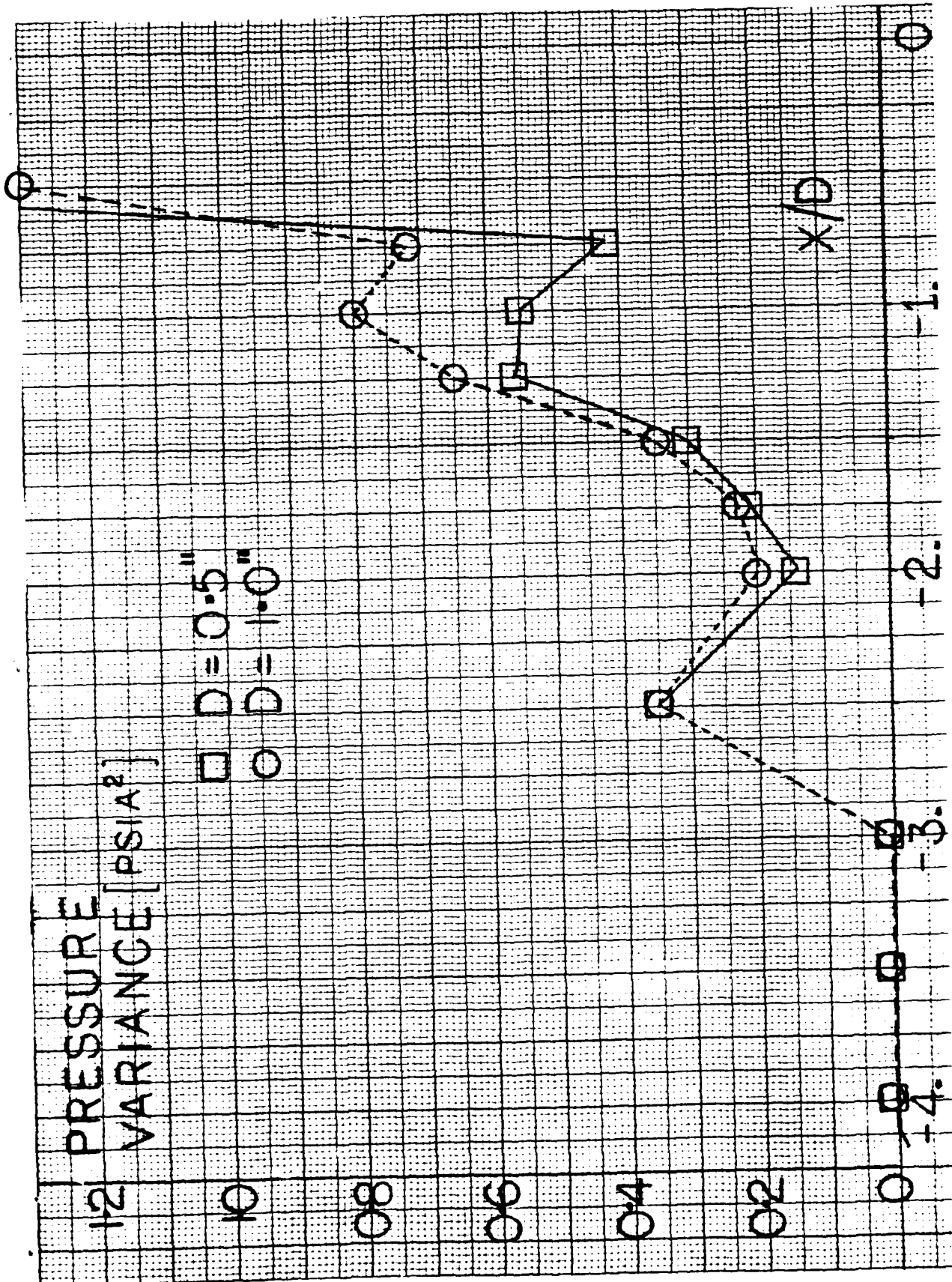


Figure 31. Variance of Pressure Fluctuations on the Plane of Symmetry Ahead of Two Different Diameter Blunt Fins

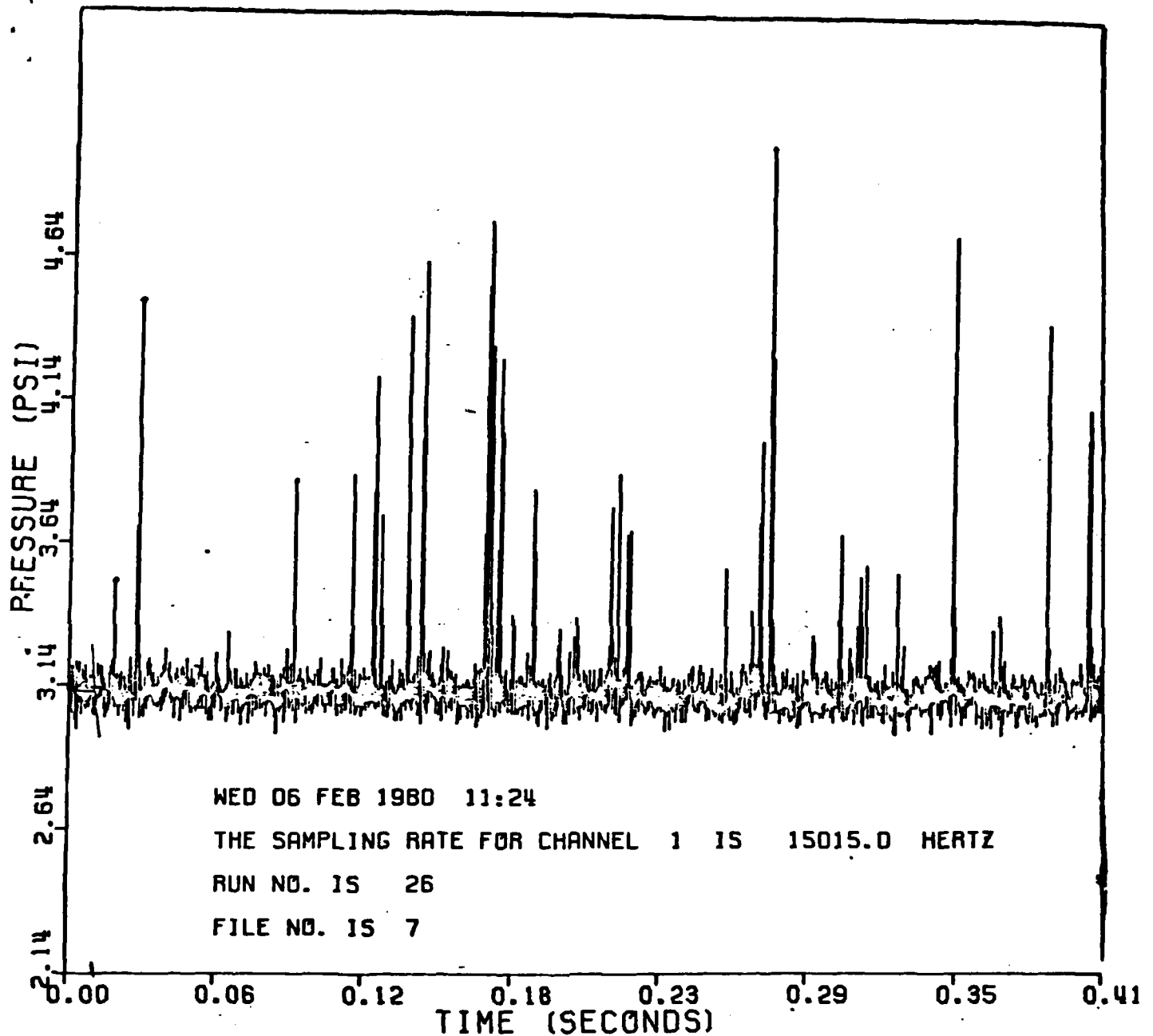


Figure 32. Surface Pressure Time History on Plane of Symmetry
2.9D Ahead of Fin Leading Edge